CZECH TECHNICAL UNIVERSITY IN PRAGUE
Faculty of Electrical Engineering
Department of Control Engineering

Algorithms for Advanced Motion Control Using Permanent Magnet Synchronous Motors and Brushless DC Motors

Master's thesis

Lukáš Černý

Supervisor
doc. Ing. Zdeněk Hurák, Ph.D.

2020

MASTER'S THESIS ASSIGNMENT

I. Personal and study details

Student's name: **Černý Lukáš** Personal ID number: **434810**

Faculty / Institute: **Faculty of Electrical Engineering**

Department / Institute: **Department of Control Engineering**

Study program: **Cybernetics and Robotics**

Branch of study: **Cybernetics and Robotics**

II. Master's thesis details

Master's thesis title in English:

Algorithms for advanced motion control using permanent magnet synchronous motors and brushless DC motors

Master's thesis title in Czech:

Algoritmy pro pokročilé řízení polohy pomocí synchronních motorů s permanentním magnetem a bezkartáčových stejnosměrných motorů

Guidelines:

The goal of the project is to demonstrate the use of some advanced algorithms for position control for PMSM and BLDC motors. In particular the algorithms for model predictive control (MPC) will be studied.
1. Describe the essentials of PMSM motors and create a simulation model. Explain the difference between the PMSM and BLDC motors.
2. Explain the basic concepts and principles relevant for motion (position) control using these motors.
3. Provide a survey of approaches to model predictive control for these motors.
4. Choose one or two approaches and do the design. Verify if using numerical simulations.
5. Choose a suitable hardware platform for implementation of prototype algorithms taking into consideration the need to performa numerical optimization in real time.
6. Demonstrate the functionality of the designed and implemented algorithm(s) using a laboratory experiment.

Bibliography / sources:

[1] T. Geyer, Model Predictive Control of High Power Converters and Industrial Drives. Wiley, 2016.
[2] J. Chiasson, Modeling and High Performance Control of Electric Machines. Hoboken, Wiley-IEEE Press, 2005.
[3] J. Rodriguez a P. Cortes, Predictive Control of Power Converters and Electrical Drives. Wiley-IEEE Press, 2012.

Name and workplace of master's thesis supervisor:

doc. Ing. Zdeněk Hurák, Ph.D., Department of Control Engineering, FEE

Name and workplace of second master's thesis supervisor or consultant:

Date of master's thesis assignment: **07.02.2020** Deadline for master's thesis submission: **14.08.2020**

Assignment valid until: **30.09.2021**

doc. Ing. Zdeněk Hurák, Ph.D.	prof. Ing. Michael Šebek, DrSc.	prof. Mgr. Petr Páta, Ph.D.
Supervisor's signature	Head of department's signature	Dean's signature

© ČVUT v Praze, Design: ČVUT v Praze, VIC

Declaration

I hereby declare that this thesis is my original work and it has been written by me in its entirety. I have duly acknowledged all the sources of information which have been used in the thesis. This thesis has also not been submitted for any degree in any university previously.

Lukáš Černý
August 2020

Acknowledgements

I would like to sincerely thank my supervisor for his help and support, and my parents for their care. I would also like to honestly thank my brother and sister. Special thanks go to Katka, Honza, Jan, Pepa, and Vítek.

Thank you.

Abstract

This thesis is concerned with the control of position, velocity, and torque in permanent magnet synchronous motors. The mathematical model of a synchronous motor is thoroughly described and then simplified to a linear model used by model predictive control methods. Then, three types of control algorithms are described including the classical field-oriented PI controller, model predictive control, and finite-control-set model predictive control. In case of the predictive methods, both single-loop and cascaded multi-loop structures are considered. The described methods are then evaluated in simulation.

Keywords: Permanent magnet synchronous motor, PMSM, brushless DC motor, BLDC, model predictive control, MPC, finite-control-set model predictive control, FCS-MPC

Abstrakt

Tato práce se zabývá řízením polohy, rychlosti a momentu síly synchronních motorů s permanentním magnetem. Matematický model synchronního motoru je důkladně popsán a na jeho základě je odvozen zjednodušený lineární model použitý pro prediktivní řízení. Poté jsou popsány tři typy řídicích algoritmů zahrnující klasické vektorové řízení pomocí PI regulátoru, prediktivní řízení a prediktivní řízení s uvažováním diskrétních aktuátorů známé jako finite-control-set MPC. U prediktivních metod je uvažována kaskádní i jednoregulátorová struktura. Popsané metody jsou ověřeny v simulaci a následně zhodnoceny.

Klíčová slova: Synchronní motor s permanentním magnetem, PMSM, bezkartáčový DC motor, BLDC, prediktivní řízení, MPC, FCS-MPC

Contents

Acronyms

BLDC	brushless DC
CCS-MPC	continuous-control-set MPC
DC	direct current
DTC	direct torque control
EMF	electromotive force
FCS-MPC	finite-control-set MPC
FPGA	field-programmable gate array
HIL	hardware in the loop
IPMSM	interior PMSM
MIMO	multi-input, multi-output
MPC	model-predictive control
PI	proportional-integral
PID	proportional-integral-derivative
PMSM	permanent-magnet synchronous motor
PWM	pulse-width modulation
RMS	root mean square

SISO	single-input, single-output
SoC	system on a chip
SPMSM	surface-mounted PMSM
SVM	space-vector modulation

Chapter 1

Introduction

Permanent-magnet synchronous motors (PMSMs) and brushless DC (BLDC) motors are three-phase motors with permanent magnets on the rotor and the phase windings on the stator, which makes the motor construction commutator-free. The absence of commutator ensures energy efficiency and mechanical simplicity, and thus makes these motors more reliable than their brushed counterparts as there are fewer components that may wear out. PMSMs and BLDC motors also have a relatively high torque-to-volume ratio [1]. Another advantage is that they allow for reducing the magnitude of the magnetic field inside the motor by means of a technique known as field weakening, which in turn enables operation at higher speeds. For these reasons, PMSMs and BLDC motors are a suitable option for torque, velocity, or position control in many industrial applications.

The advantages of PMSMs and BLDC motors come at the cost of the increased complexity of control methods. The commutation, i.e., the process of varying currents through individual phases, is realized electrically without an electromechanical commutator. Usually, a three-phase inverter is employed together with a digital controller that operates the switching elements in the inverter. The digital controller must operate at a sufficiently high frequency determined primarily by the motor parameters and the requirements on the precision of control.

Many PMSM/BLDC motor control algorithms neglect the switching nature of the inverter and generate three phase voltages in the form of three real numbers. The generated numbers are then translated into two-state signals driving the switching elements in the inverter. The translation utilizes a modulation scheme such as pulse-width modulation (PWM) or space-vector modulation (SVM). These algorithms include scalar control and field-oriented proportional-integral-derivative (PID) controller.

There is another class of control algorithms that take the switching nature into account and generate two-state signals directly. Direct torque control (DTC) is an example. Another example is a combination of DTC and model-predictive control (MPC) called FCS-MPC. It formulates the control task as an optimization problem with binary decision variables, a problem belonging to the class of integer programs. In this context, MPC with real-valued decision variables is sometimes referred to as CCS-MPC [2], [3].

FCS-MPC and CCS-MPC provide a framework to deal with the control of, possibly nonlinear, constrained multi-input, multi-output (MIMO) systems. They both find optimal control over a finite time horizon with the possibility to take into consideration time-varying reference. All these advantages can be exploited to control PMSMs and BLDC motors.

Also, a subtle selection of the cost function in an MPC algorithm can result in an inherent flux weakening at higher speeds. When compared to continuous-control-set algorithms, FCS-MPC may yield an improved performance provided that it operates at a significantly higher frequency. Higher sampling frequency does not necessarily mean higher switching frequency, but it provides the controller more options to select optimal time instants for the switching events. In fact, FCS-MPC provides a convenient way to select a trade-off between the performance and the maximum switching frequency. Low switching frequencies usually yield significant torque ripple whereas high switching frequencies yield smoother torque. On the other hand, high switching frequencies are also associated with significant power losses. FCS-MPC does not keep fixed switching frequency, unlike in the case of algorithms using modulators. In some applications, this is considered a problem because of the possibility of low-order harmonics being propagated into the grid [4]. FCS-MPC is often implemented using very short control horizons of length 1 or 2. The reasons are high sampling frequency and the computational burden of finding the optimal solution, which grows exponentially with the length of the prediction horizon.

This thesis describes the following control algorithms for PMSMs presented in the available literature: field-oriented proportional-integral (PI) controller, CCS-MPC, and FCS-MPC. The algorithms were tested in simulation and both single-loop and multi-loop cascaded structures were analyzed. The tests examined the ability to track torque, velocity, and position references under no-load conditions and with an external load torque. Suitable platform for hardware implementation was chosen, however, verification of the algorithms on an actual PMSM have not been done yet. All simulation files are provided in the attachment to this thesis.

1.1 Classification of Electric Motors

A possible classification of the basic types of electric motors based on the principle of their operation is given in [5] and is shown in fig. 1.1.

Perhaps the simplest and the easiest to control are permanent magnet DC motors. Specifically, the application of constant voltage results in constant steady-state velocity. When the stator permanent magnets are replaced by controlled winding, one gains an extra degree of freedom, which allows for field weakening. Such motors are called separately excited DC motors. The main drawback of DC motors is the presence of commutator, which makes them less efficient than PMSMs and BLDC motors.

Induction motors are more similar to PMSMs and BLDC motors. The difference is that induction motors do not have permanent magnets on the rotor. Instead, the rotor is made of soft magnetic material that enables the induction of rotor currents by commutating the stator currents. Such a design requires asynchronous operation. In other words, the rotor is required to rotate at a different velocity than the magnetic field generated by the stator and the difference determines the generated torque. For high-performance control, the induced rotor currents must be estimated. Thus, control of induction motors is slightly more complicated

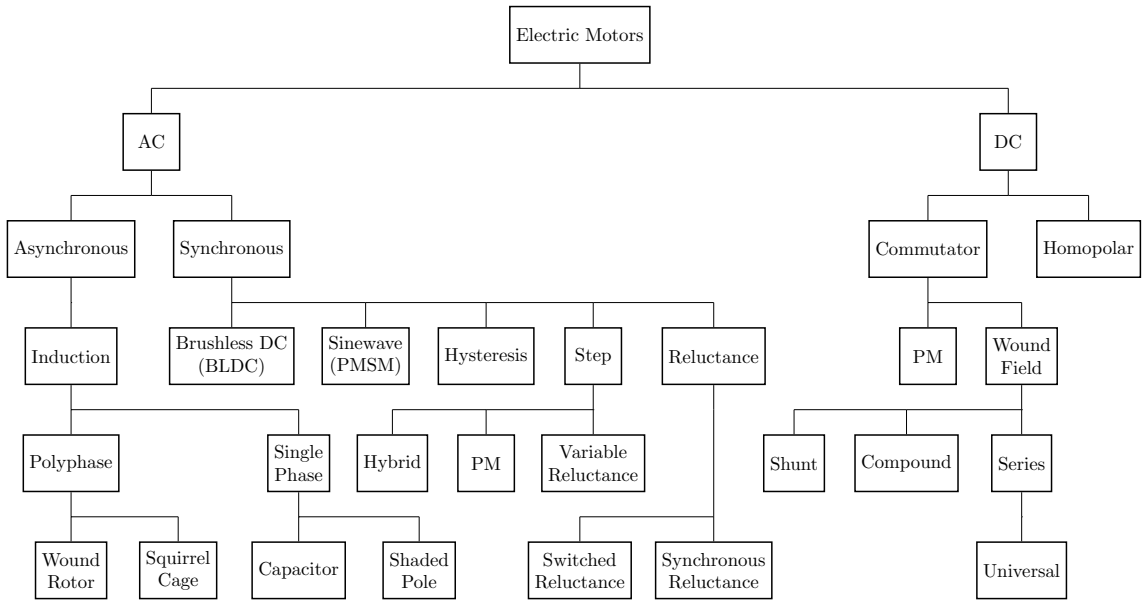

Figure 1.1: Classification of electric motors. Adapted with permission from [5, Figure 1.1].

than control of PMSMs and BLDC motors.

Permanent-magnet stepper motors are very similar to PMSMs and BLDC motors. As shown in [6], their mathematical model is identical to the two-phase equivalent model of PMSM, and therefore the same control algorithms may be applied. A high number of pole pairs in the stepper motors makes open-loop position control reasonably precise. Nonetheless, closed-loop feedback control greatly improves performance and efficiency.

The difference between PMSMs and BLDC motors is in the back electromotive force (EMF), i.e., the voltage[1] induced in the phase windings by the rotating permanent magnets. PMSMs have a sinusoidal shape of the back EMF at the constant speed, whereas in the case of BLDC motors, the shape is trapezoidal [6]. The trapezoidal shape makes the motors suitable for six-step operation [7], which is easy and cheap to implement. The reason BLDC motors are called brushless DC is that they often come with a current controller, and the overall closed-loop system can be controlled in a similar way as a DC motor [6]. It is worth noting that some texts do not make the distinction between PMSMs and BLDC motors, e.g. [1]. Also, some PMSMs and BLDC motors have neither sinusoidal nor trapezoidal shape of the back EMF and the shape is described by more general periodic function. Control of such motors is addressed in [8].

[1]Here, no distinction between voltage and EMF is made based on the remark in [6, Section 1.5.1].

1.2 Related Work

Now, a short list of relevant work done by others is given. A comprehensive overview of CCS-MPC and FCS-MPC algorithms applied in different areas of power electronics is given in [4]. A possible implementation of CCS-MPC for PMSM with hardware in the loop (HIL) verification was presented by authors of [2]. A comparison of FCS-MPC and CCS-MPC is given in [3], where both algorithms showed similar results. An overview focused on FCS-MPC is given in [9]. A detailed description of one-step FCS-MPC implementations used for different topologies of power converters is given in [10]. Several variants of FCS-MPC with a long prediction horizon designed for medium-voltage induction motors are described in [11]. Also, the author of [11] shows that FCS-MPC applied to a three-level power converter can both reduce the switching losses and improve the performance at the same time when compared to algorithms with voltage modulation stage. In contrast, in this thesis, FCS-MPC is designed for low-voltage PMSM with a two-level inverter.

Chapter 2

Permanent Magnet Synchronous Motors

This chapter describes the principle of the operation of a PMSM and the mathematical model. The model is then transformed into a two-phase equivalent model using the Clarke transformation. Further, the DQ model is obtained using the Park transformation, which is then linearized and discretized. Then, model parameters are discussed. Finally, constraints on the inputs and state variables are addressed. For a rigorous derivation of the model, the reader is referred to [6] and [1]. Also, the model of a BLDC motor can be found in [6].

2.1 Principle of Operation

Fig. 2.1(a) shows the basic idea of the operation of a PMSM. The motor consists of three stator phases, usually denoted as A, B, and C, and a permanent magnet on the rotor. Each of the three phases consists of two coils that generate a magnetic field when current is running through them. The orientation of the magnetic field around each coil is determined by the direction of the current. The figure depicts the orientation for a given situation by N (for North pole) and S (for South pole). The stator magnetic poles attract opposite rotor poles and create torque. The stator currents are varied such that the created torque turns the rotor in the desired direction. At constant rotor speed and constant external load torque, the optimal phase currents are of sinusoidal shape, as a function of time, as shown in fig. 2.1(b). Such current waveforms produce constant torque that compensates for the load torque and friction. The optimal shape is a result of the sinusoidal shape of back EMFs, which is a result of the actual motor construction and geometry.

Although a typical PMSM consists of three phases, the number may be different. The same applies to the number of coils per phase and the number of rotor magnets. The phase windings are not necessarily solenoidal, as in fig. 2.1(a). Instead, they can be distributed around the stator perimeter. Also, the rotor magnets may be either inside the stator, as in fig. 2.1(a), or outside. Such configurations are called interior PMSM (IPMSM) and surface-mounted PMSM (SPMSM), respectively. Usually, the three phases are not controlled independently but, rather, they are connected together in a star or delta configuration, which are depicted in fig. 2.2. Both configurations reduce the number of wires connected to the motor and make it a three-terminal device.

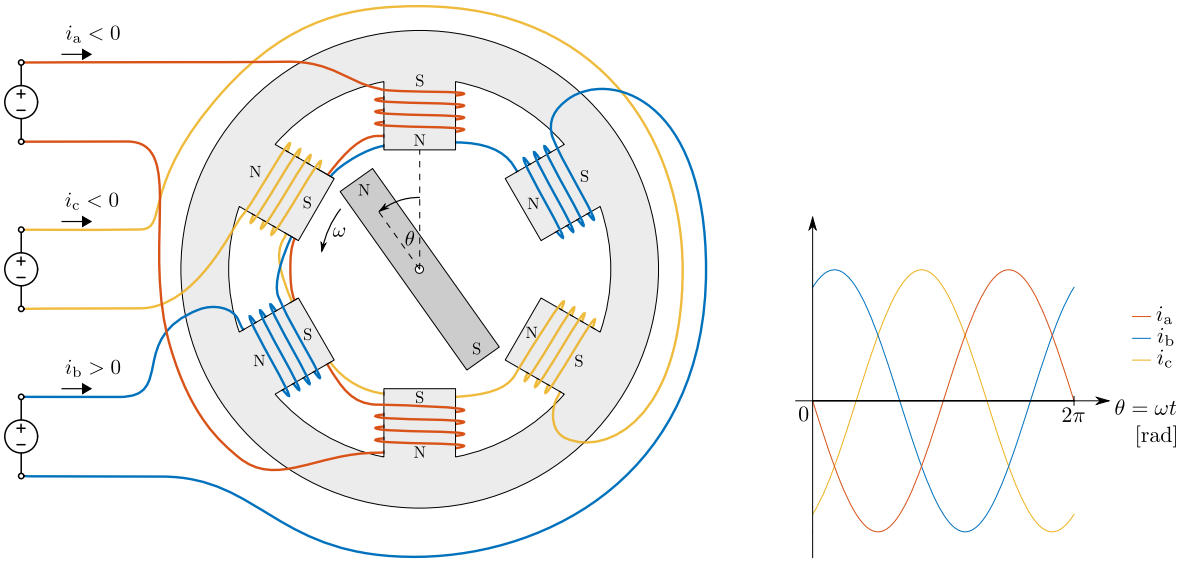

(a) Principle of operation of PMSM. **(b)** Optimal current waveforms.

Figure 2.1: Principle of operation of PMSM (a) and optimal current waveforms at constant speed and constant load torque (b). The three phases A, B, and C are represented by red, blue, and yellow colors, respectively.

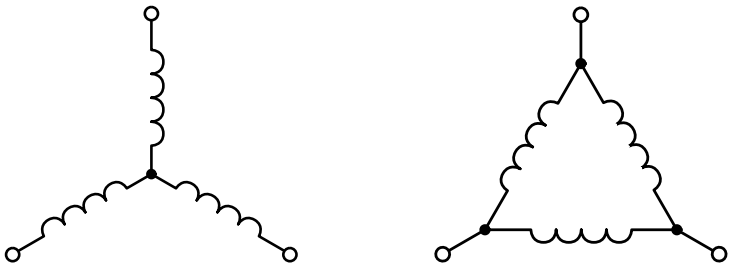

(a) Star configuration. **(b)** Delta configuration.

Figure 2.2: Two common configurations of PMSM phase windings.

2.2 Mathematical model

2.2.1 Assumptions

The following mathematical model was derived making certain assumptions. Firstly, the motor is assumed to be a three-phase symmetrical PMSM. In other words, all three phases have the same properties and the only difference is that they are rotated in space by 120 degrees with respect to each other, and the motor geometry is such that the back EMFs are of sinusoidal shape. Secondly, it is assumed that the motor is made of ideal linear magnetic materials and that there are no losses in the magnetic circuit. Hence, effects such as magnetic saturation of the materials, hysteresis of B-H curve, and eddy-current losses are not considered. Also, the model parameters are assumed to be constant, whereas in reality they can vary significantly due to temperature rise in the motor and due to magnetic saturation.

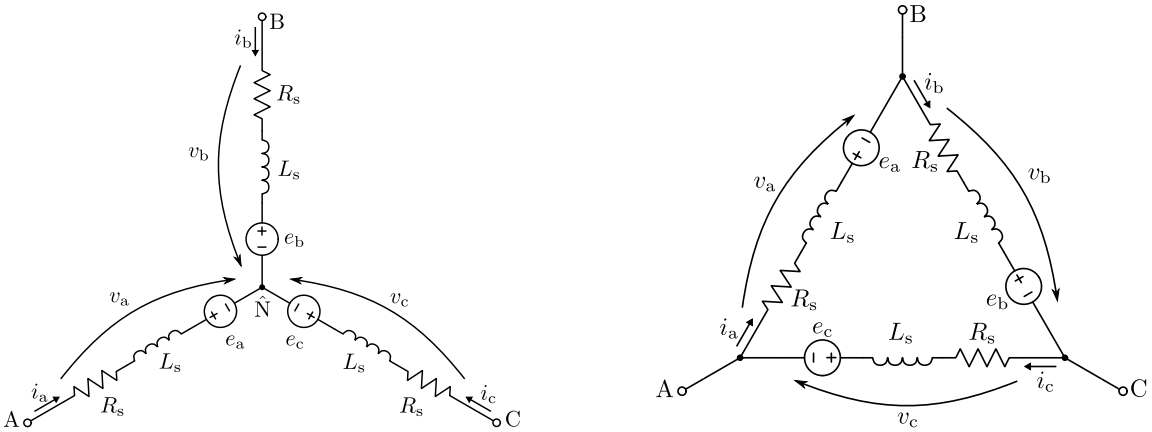

(a) Star configuration. **(b)** Delta configuration.

Figure 2.3: Model of electrical part of PMSM (the voltage arrows are oriented toward the reference point).

2.2.2 Definition of Rotor Angle

As depicted in fig. 2.1(a), the rotor angle θ is defined to be the angle between the magnetic axes of the rotor magnet and phase A. This implies that positive current through phase A creates torque that attracts the rotor to zero angle. The orientation is such that phase B is rotated in space by 120 degrees from phase A and phase C is rotated by 240 degrees (or -120 degrees) from phase A. The angular velocity is

$$\omega \;=\; \frac{\mathrm{d}\theta}{\mathrm{d}t}. \tag{2.1}$$

When there are more coils per phase and/or more rotor magnets, there are more possibilities to choose zero angle according to the above definition as the rotor and/or phase A have more than one magnetic axis. In such case, any position at which the magnetic axes are aligned is picked as zero angle. The effects of the rotor position on the phase windings are periodic functions of θ with period $2\pi/n_{\mathrm{pp}}$, where n_{pp} is the number of pole pairs on the stator and the rotor.

2.2.3 Voltage Equations

Fig. 2.3 shows model of electrical part of PMSM in star and delta configurations. In both cases, the phase voltages v_{a}, v_{b}, and v_{c} are expressed in terms of the phase currents i_{a}, i_{b}, i_{c} and the total flux linkage in each phase ψ_{a}, ψ_{b}, ψ_{c} as

$$\boldsymbol{v}_{\mathrm{abc}} \;=\; R_{\mathrm{s}}\boldsymbol{i}_{\mathrm{abc}} + \frac{\mathrm{d}}{\mathrm{d}t}\boldsymbol{\psi}_{\mathrm{abc}}, \tag{2.2}$$

where

$$\boldsymbol{v}_{\mathrm{abc}} = \begin{bmatrix} v_{\mathrm{a}} \\ v_{\mathrm{b}} \\ v_{\mathrm{c}} \end{bmatrix}, \quad \boldsymbol{i}_{\mathrm{abc}} = \begin{bmatrix} i_{\mathrm{a}} \\ i_{\mathrm{b}} \\ i_{\mathrm{c}} \end{bmatrix}, \quad \boldsymbol{\psi}_{\mathrm{abc}} = \begin{bmatrix} \psi_{\mathrm{a}} \\ \psi_{\mathrm{b}} \\ \psi_{\mathrm{c}} \end{bmatrix}, \tag{2.3}$$

and R_{s} is phase resistance. The flux linkages consist of two components

$$\boldsymbol{\psi}_{\mathrm{abc}} \;=\; \boldsymbol{\psi}_{\mathrm{abcs}} + \boldsymbol{\psi}_{\mathrm{abcr}}, \tag{2.4}$$

where $\boldsymbol{\psi}_{\mathrm{abcs}} = \begin{bmatrix} \psi_{\mathrm{as}} & \psi_{\mathrm{bs}} & \psi_{\mathrm{cs}} \end{bmatrix}^{\mathrm{T}}$ are the components of the flux linkages due to the stator currents and $\boldsymbol{\psi}_{\mathrm{abcr}} = \begin{bmatrix} \psi_{\mathrm{ar}} & \psi_{\mathrm{br}} & \psi_{\mathrm{cr}} \end{bmatrix}^{\mathrm{T}}$ are the components of the flux linkages due to the rotor magnets. The components of the flux linkages due to the stator currents are

$$\boldsymbol{\psi}_{\mathrm{abcs}} \;=\; \boldsymbol{L}\boldsymbol{i}_{\mathrm{abc}} \tag{2.5}$$

with $\boldsymbol{L}$ being the inductance matrix. If the air gap between the stator and rotor is uniform, self-inductance of each phase L_{s} and mutual inductance between each two phases $-M_{\mathrm{s}}$ are constant and the inductance matrix is

$$\boldsymbol{L}_{\mathrm{uniform}} \;=\; \begin{bmatrix} L_{\mathrm{s}} & -M_{\mathrm{s}} & -M_{\mathrm{s}} \\ -M_{\mathrm{s}} & L_{\mathrm{s}} & -M_{\mathrm{s}} \\ -M_{\mathrm{s}} & -M_{\mathrm{s}} & L_{\mathrm{s}} \end{bmatrix}. \tag{2.6}$$

The negative signs at the mutual inductances are due to the phases being rotated with respect to each other by 120 degrees and, thus, positive current in a phase winding induces negative currents in the other two phases. If the motor has salient poles and the air gap is non-uniform, the inductances vary with the rotor angle. The changes in the inductances can be approximated as

$$\boldsymbol{L} \;=\; \boldsymbol{L}_{\mathrm{uniform}} + L_{\mathrm{g}} \begin{bmatrix} \cos 2\left(n_{\mathrm{pp}}\theta\right) & \cos 2\left(n_{\mathrm{pp}}\theta - \frac{\pi}{3}\right) & \cos 2\left(n_{\mathrm{pp}}\theta + \frac{\pi}{3}\right) \\ \cos 2\left(n_{\mathrm{pp}}\theta - \frac{\pi}{3}\right) & \cos 2\left(n_{\mathrm{pp}}\theta - \frac{2\pi}{3}\right) & \cos 2\left(n_{\mathrm{pp}}\theta\right) \\ \cos 2\left(n_{\mathrm{pp}}\theta + \frac{\pi}{3}\right) & \cos 2\left(n_{\mathrm{pp}}\theta\right) & \cos 2\left(n_{\mathrm{pp}}\theta + \frac{2\pi}{3}\right) \end{bmatrix}, \tag{2.7}$$

where the constant inductance matrix $\boldsymbol{L}_{\mathrm{uniform}}$ is used to represent the mean inductances and L_{g} is the amplitude of the changes in inductance. The fluctuations are periodic functions with period π/n_{pp}, which corresponds to the fact that the inductances are not affected by the rotor magnetic field and, hence, the polarity of the rotor magnets does not matter. It is

assumed that flux linkages due to rotor magnets are

$$\boldsymbol{\psi}_{\mathrm{abcr}} \;=\; \Psi_{\mathrm{m}} \begin{bmatrix} \cos\left(n_{\mathrm{pp}}\theta\right) \\ \cos\left(n_{\mathrm{pp}}\theta - \frac{2\pi}{3}\right) \\ \cos\left(n_{\mathrm{pp}}\theta + \frac{2\pi}{3}\right) \end{bmatrix}, \tag{2.8}$$

where Ψ_{m} denotes the amplitude of the components of $\boldsymbol{\psi}_{\mathrm{abcr}}$. The back EMFs in each phase are then[1]

$$\boldsymbol{e}_{\mathrm{abc}} \;=\; \begin{bmatrix} e_{\mathrm{a}} \\ e_{\mathrm{b}} \\ e_{\mathrm{c}} \end{bmatrix} \;=\; \frac{\mathrm{d}}{\mathrm{d}t}\boldsymbol{\psi}_{\mathrm{abcr}} \;=\; -n_{\mathrm{pp}}\omega\,\Psi_{\mathrm{m}} \begin{bmatrix} \sin\left(n_{\mathrm{pp}}\theta\right) \\ \sin\left(n_{\mathrm{pp}}\theta - \frac{2\pi}{3}\right) \\ \sin\left(n_{\mathrm{pp}}\theta + \frac{2\pi}{3}\right) \end{bmatrix}. \tag{2.9}$$

Using (2.4), (2.5) and (2.9), the phase voltages $\boldsymbol{v}_{\mathrm{abc}}$ are expressed as

$$\boldsymbol{v}_{\mathrm{abc}} \;=\; R_{\mathrm{s}}\boldsymbol{i}_{\mathrm{abc}} + \boldsymbol{L}\frac{\mathrm{d}\boldsymbol{i}_{\mathrm{abc}}}{\mathrm{d}t} + \omega\frac{\partial \boldsymbol{L}}{\partial\theta}\boldsymbol{i}_{\mathrm{abc}} + \boldsymbol{e}_{\mathrm{abc}}. \tag{2.10}$$

where the effects of the magnetic field of the rotor magnets are contained in the back EMF term.

2.2.4 Balanced Conditions

In a star-connected PMSM, Kirchhoff's current law applied at the motor neutral point $\hat{\mathrm{N}}$ states that the phase currents are balanced and satisfy

$$i_{\mathrm{a}} + i_{\mathrm{b}} + i_{\mathrm{c}} \;=\; 0. \tag{2.11}$$

From (2.5) and (2.7) it follows that

$$\psi_{\mathrm{as}} + \psi_{\mathrm{bs}} + \psi_{\mathrm{cs}} \;=\; 0. \tag{2.12}$$

The sinusoidal shape of flux linkages due to rotor magnets given by (2.8) implies

$$\psi_{\mathrm{ar}} + \psi_{\mathrm{br}} + \psi_{\mathrm{cr}} \;=\; 0 \tag{2.13}$$

and as a result

$$v_{\mathrm{a}} + v_{\mathrm{b}} + v_{\mathrm{c}} \;=\; 0. \tag{2.14}$$

[1] Some texts use different sign convention and define the back EMFs to be the negative of the expression in (2.9). The sign conventions used here is, however, more common [6].

Put into words, the phase voltages are also balanced.

In a delta-connected PMSM, Kirchhoff's voltage law applied to the phase voltages states that they are balanced and satisfy

$$v_\mathrm{a} + v_\mathrm{b} + v_\mathrm{c} \;=\; 0. \tag{2.15}$$

The sinusoidal shape of back EMFs given by (2.9) implies

$$e_\mathrm{a} + e_\mathrm{b} + e_\mathrm{c} \;=\; 0. \tag{2.16}$$

Therefore, summing up the equations in (2.10) gives

$$0 \;=\; R_\mathrm{s} i_\mathrm{zs} + (L_\mathrm{s} - 2M_\mathrm{s})\frac{\mathrm{d}}{\mathrm{d}t} i_\mathrm{zs}, \tag{2.17}$$

where

$$i_\mathrm{zs} \;=\; \frac{1}{3}(i_\mathrm{a} + i_\mathrm{b} + i_\mathrm{c}) \tag{2.18}$$

is the zero-sequence (also called common-mode) current. This is the common component of the phase currents which is running in circle in the delta-connected PMSM. Under ideal conditions, there are no voltages in (2.17) that would drive the zero-sequence current and for this reason

$$i_\mathrm{zs} \;=\; 0. \tag{2.19}$$

Thus, the phase currents are balanced and

$$i_\mathrm{a} + i_\mathrm{b} + i_\mathrm{c} \;=\; 0. \tag{2.20}$$

In practice, the zero-sequence current might be nonzero due to imbalance and asymmetry in the motor. For example, if the back EMFs are non-sinusoidal and contain triplen harmonics (as in case of BLDC motors), they are not balanced and the common-mode back EMF drives the zero-sequence current. However, in delta-connected PMSMs i_zs is usually negligible.

2.2.5 Relationship Between Phase and Source Variables

The voltage equations given in section 2.2.3 are in terms of the phase voltages $\boldsymbol{v}_\mathrm{abc}$ and phase currents $\boldsymbol{i}_\mathrm{abc}$. The manipulated variables are, however, the source voltages

$$\boldsymbol{v}_\mathrm{abcs} \;=\; \begin{bmatrix} v_\mathrm{as} & v_\mathrm{bs} & v_\mathrm{cs} \end{bmatrix}^\mathrm{T} \tag{2.21}$$

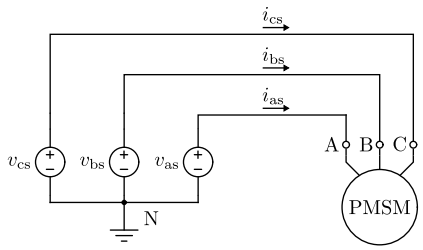

Figure 2.4: PMSM connected to a three-phase voltage source.

and the currents drawn from the three-phase power supply are the source currents

$$\boldsymbol{i}_{\mathrm{abcs}} = \begin{bmatrix} i_{\mathrm{as}} & i_{\mathrm{bs}} & i_{\mathrm{cs}} \end{bmatrix}^{\mathrm{T}}. \tag{2.22}$$

This is shown in fig. 2.4. The relationship between the phase variables and the source variables is now given.

In star-connected PMSM, the phase voltages $\boldsymbol{v}_{\mathrm{abc}}$ are taken with respect to the motor neutral point $\hat{\mathrm{N}}$. The source voltages v_{as}, v_{bs}, v_{cs} are taken with respect to the source neutral point N. The relationship between the two sets of voltages is

$$v_{\mathrm{as}} = v_{\mathrm{a}} + v_{\hat{\mathrm{n}}\mathrm{n}}, \tag{2.23}$$

$$v_{\mathrm{bs}} = v_{\mathrm{b}} + v_{\hat{\mathrm{n}}\mathrm{n}}, \tag{2.24}$$

$$v_{\mathrm{cs}} = v_{\mathrm{c}} + v_{\hat{\mathrm{n}}\mathrm{n}} \tag{2.25}$$

where $v_{\hat{\mathrm{n}}\mathrm{n}}$ is the voltage at the motor neutral point $\hat{\mathrm{N}}$ with respect to the source neutral point N. Summing up these three equations and using the balanced conditions of v_{a}, v_{b}, and v_{c} gives

$$v_{\hat{\mathrm{n}}\mathrm{n}} = \frac{1}{3}\left(v_{\mathrm{as}} + v_{\mathrm{bs}} + v_{\mathrm{cs}}\right). \tag{2.26}$$

Thus, the voltage between the two neutral points $v_{\hat{\mathrm{n}}\mathrm{n}}$ is equal to the common-mode voltage of the three source voltages. The source voltages need not to be balanced and, therefore, the common-mode voltage $v_{\hat{\mathrm{n}}\mathrm{n}}$ may be chosen non-zero. However, $v_{\hat{\mathrm{n}}\mathrm{n}}$ does not drive the phase currents because the phase voltages v_{a}, v_{b}, and v_{c} are obtained from the source voltages by substracting $v_{\hat{\mathrm{n}}\mathrm{n}}$. In other words, only the differential modes of the source voltages drive the phase currents and the common-mode voltage can be chosen arbitrarily. For example, when the limits on the maximum and minimum source voltage are considered, the common-mode can be used to shift the source voltages such that the voltage range is fully utilized. The phase currents in star-connected PMSM are equal to the source currents

$$\boldsymbol{i}_{\mathrm{abcs}} = \boldsymbol{i}_{\mathrm{abc}}. \tag{2.27}$$

In delta-connected PMSM, the phase voltages $\boldsymbol{v}_{\mathrm{abc}}$ are the line-to-line voltages

$$v_{\mathrm{a}} = v_{\mathrm{as}} - v_{\mathrm{bs}}, \tag{2.28}$$
$$v_{\mathrm{b}} = v_{\mathrm{bs}} - v_{\mathrm{cs}}, \tag{2.29}$$
$$v_{\mathrm{c}} = v_{\mathrm{cs}} - v_{\mathrm{as}}. \tag{2.30}$$

The inverse relationship is

$$v_{\mathrm{as}} = \frac{1}{3}(v_{\mathrm{a}} - v_{\mathrm{c}}) + v_{\mathrm{cms}}, \tag{2.31}$$
$$v_{\mathrm{bs}} = \frac{1}{3}(v_{\mathrm{b}} - v_{\mathrm{a}}) + v_{\mathrm{cms}}, \tag{2.32}$$
$$v_{\mathrm{cs}} = \frac{1}{3}(v_{\mathrm{c}} - v_{\mathrm{b}}) + v_{\mathrm{cms}}, \tag{2.33}$$

where

$$v_{\mathrm{cms}} = \frac{1}{3}(v_{\mathrm{as}} + v_{\mathrm{bs}} + v_{\mathrm{cs}}) \tag{2.34}$$

is the common-mode voltage of the source voltages. As the phase voltages are line-to-line, they do not depend on the common mode of the source voltages and v_{cms} can be chosen arbitrarily as in case of star-connected PMSM. Applying Kirchhoff's current law at each terminal of delta-connected PMSM gives

$$i_{\mathrm{as}} = i_{\mathrm{a}} - i_{\mathrm{c}}, \tag{2.35}$$
$$i_{\mathrm{bs}} = i_{\mathrm{b}} - i_{\mathrm{a}}, \tag{2.36}$$
$$i_{\mathrm{cs}} = i_{\mathrm{c}} - i_{\mathrm{b}}. \tag{2.37}$$

The inverse relationship is obtained using the balanced conditions of the phase currents as

$$i_{\mathrm{a}} = \frac{1}{3}(i_{\mathrm{as}} - i_{\mathrm{bs}}), \tag{2.38}$$
$$i_{\mathrm{b}} = \frac{1}{3}(i_{\mathrm{bs}} - i_{\mathrm{cs}}), \tag{2.39}$$
$$i_{\mathrm{c}} = \frac{1}{3}(i_{\mathrm{cs}} - i_{\mathrm{as}}). \tag{2.40}$$

When the source currents are measured, the above transformation is required to obtain the phase currents. Similarly, when given phase voltages are to be applied, they should be transformed to obtain required source voltages. These transformations can be avoided by transforming motor parameters to star-connected PMSM equivalent parameters and by changing the definition of the rotor angle. By doing so, one can treat delta-connected PMSM in the same way as star-connected PMSM. Details are provided in appendix A.

In practice, a PMSM is driven by an inverter connected to a DC power supply. Fig. 2.5 shows PMSM connected to a simplified model of an inverter. Although one usually uses a

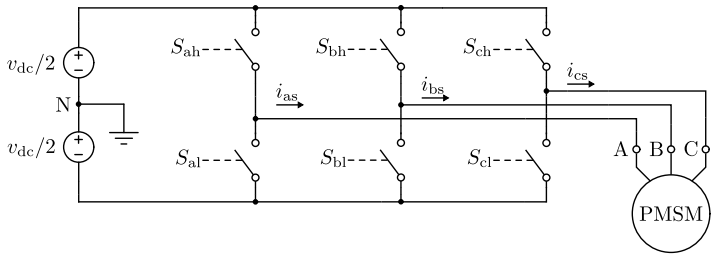

Figure 2.5: PMSM connected to a simplified model of an inverter.

single DC power supply that provides v_{dc} voltage between its terminals with one terminal being the neutral, it is convenient to choose the source neutral point N in between as in fig. 2.5. The control signals S_{ah}, S_{al}, S_{bh}, S_{bl}, S_{ch}, $S_{cl} \in \{0, 1\}$ determine whether the respective switch is open or closed, and thus determine whether the respective motor phase is connected to $+v_{dc}/2$, $-v_{dc}/2$, or if it is left floating.

2.2.6 Mechanical Equation

The rotor angle is governed by

$$J\frac{\mathrm{d}\omega}{\mathrm{d}t} \;=\; \tau_{el} + \tau_{fr} + \tau_{cog} + \tau_{ex}, \tag{2.41}$$

where J is the moment of inertia of the rotor, τ_{el} is electromagnetic torque generated by the stator currents, τ_{fr} is torque due to mechanical friction, τ_{cog} is cogging torque, and τ_{ex} is external torque applied to the rotor shaft.

The friction torque is

$$\tau_{fr} \;=\; -B\omega, \tag{2.42}$$

where B is the coefficient of viscous friction.

The electromagnetic torque is derived in appendix A and it is

$$\tau_{el} \;=\; \frac{1}{2}\boldsymbol{i}_{abc}^{T}\frac{\partial \boldsymbol{L}}{\partial\theta}\boldsymbol{i}_{abc} + \frac{1}{\omega}\boldsymbol{i}_{abc}^{T}\boldsymbol{e}_{abc}. \tag{2.43}$$

The first term is called reluctance torque and the second is called synchronous torque. The reluctance torque is an effect of motor saliency and it is zero in PMSMs with uniform air gap. It can be shown that the electromagnetic torque is constant when the phase currents are sinusoidal functions of θ. Specifically, setting

$$\boldsymbol{i}_{abc} \;=\; -I_m\left[\sin\left(n_{pp}\theta\right) \quad \sin\left(n_{pp}\theta - \tfrac{2\pi}{3}\right) \quad \sin\left(n_{pp}\theta + \tfrac{2\pi}{3}\right)\right]^{T} \tag{2.44}$$

results in

$$\tau_{\mathrm{el}} \;=\; \frac{3}{2} n_{\mathrm{pp}}\, \Psi_{\mathrm{m}} I_{\mathrm{m}}. \tag{2.45}$$

Thus, the selected amplitude I_{m} of the stator currents is proportional to the generated torque. The current waveforms in (2.44) are depicted in fig. 2.1(b) for PMSM with $n_{\mathrm{pp}} = 1$. More generally, setting

$$\boldsymbol{i}_{\mathrm{abc}} \;=\; -I_{\mathrm{m}} \begin{bmatrix} \sin\left(n_{\mathrm{pp}}\theta - \phi\right) & \sin\left(n_{\mathrm{pp}}\theta - \phi - \frac{2\pi}{3}\right) & \sin\left(n_{\mathrm{pp}}\theta - \phi + \frac{2\pi}{3}\right) \end{bmatrix}^{\mathrm{T}} \tag{2.46}$$

results in

$$\tau_{\mathrm{el}} \;=\; \frac{3}{2} n_{\mathrm{pp}}\, \Psi_{\mathrm{m}} I_{\mathrm{m}} \cos\phi + \frac{9}{4} n_{\mathrm{pp}} L_{\mathrm{g}} I_{\mathrm{m}}^2 \sin(2\phi), \tag{2.47}$$

where ϕ is constant phase shift.

The cogging torque τ_{cog} is another effect of the motor saliency. It is torque that attracts the rotor to certain positions even when there are no currents running through the phase windings. Many PMSMs available on the market have a nominal value of cogging torque of 5 %–10 % of the rated torque [12]. Cogging torque does not result directly from the mathematical model used here. It can be left as an unknown component of the external torque τ_{ex}, or it can be measured and accounted for.

2.2.7 Resulting Model

The model is now summarized and written as

$$\boldsymbol{L} \frac{\mathrm{d}\boldsymbol{i}_{\mathrm{abc}}}{\mathrm{d}t} \;=\; -R_{\mathrm{s}} \boldsymbol{i}_{\mathrm{abc}} - \omega \boldsymbol{L}' \boldsymbol{i}_{\mathrm{abc}} - \boldsymbol{e}_{\mathrm{abc}} + \boldsymbol{v}_{\mathrm{abc}}, \tag{2.48}$$

$$J \frac{\mathrm{d}\omega}{\mathrm{d}t} \;=\; \frac{1}{2} \boldsymbol{i}_{\mathrm{abc}}^{\mathrm{T}} \boldsymbol{L}' \boldsymbol{i}_{\mathrm{abc}} + \frac{1}{\omega} \boldsymbol{i}_{\mathrm{abc}}^{\mathrm{T}} \boldsymbol{e}_{\mathrm{abc}} - B\omega + \tau_{\mathrm{cog}} + \tau_{\mathrm{ex}}, \tag{2.49}$$

$$\frac{\mathrm{d}\theta}{\mathrm{d}t} \;=\; \omega \tag{2.50}$$

where

$$\boldsymbol{L}' \;=\; \frac{\partial \boldsymbol{L}}{\partial \theta}. \tag{2.51}$$

From this model, the model of PMSM with uniform air gap is obtained by setting $L_{\mathrm{g}} = 0$ and $\tau_{\mathrm{cog}} = 0$.

2.3 Two-Phase Equivalent Model

The balanced conditions of three variables mean that only two of them can be chosen as independent. For this reason, only two of the three voltage equations are needed and the third state variable may be computed from (2.11). However, it is convenient to transform the equations using Clarke transformation. The transformed variables are

$$\boldsymbol{i}_{\alpha\beta\gamma} = \begin{bmatrix} i_\alpha & i_\beta & i_\gamma \end{bmatrix}^{\mathrm{T}} = \boldsymbol{K}\boldsymbol{i}_{\mathrm{abc}}, \tag{2.52}$$

$$\boldsymbol{v}_{\alpha\beta\gamma} = \begin{bmatrix} v_\alpha & v_\beta & v_\gamma \end{bmatrix}^{\mathrm{T}} = \boldsymbol{K}\boldsymbol{v}_{\mathrm{abc}}, \tag{2.53}$$

$$\boldsymbol{e}_{\alpha\beta\gamma} = \begin{bmatrix} e_\alpha & e_\beta & e_\gamma \end{bmatrix}^{\mathrm{T}} = \boldsymbol{K}\boldsymbol{e}_{\mathrm{abc}}, \tag{2.54}$$

where the transformation matrix K is defined as

$$\boldsymbol{K} = \frac{2}{3}\begin{bmatrix} 1 & -\frac{1}{2} & -\frac{1}{2} \\ 0 & \frac{\sqrt{3}}{2} & -\frac{\sqrt{3}}{2} \\ \frac{1}{2} & \frac{1}{2} & \frac{1}{2} \end{bmatrix} \tag{2.55}$$

with inverse matrix

$$\boldsymbol{K}^{-1} = \begin{bmatrix} 1 & 0 & 1 \\ -\frac{1}{2} & \frac{\sqrt{3}}{2} & 1 \\ -\frac{1}{2} & -\frac{\sqrt{3}}{2} & 1 \end{bmatrix}. \tag{2.56}$$

The first two components of the transformed vectors, α and β, are two differential modes and the third component, γ, is common mode of the abc varibles. Due to the balanced conditions, the γ components are always zero. The voltage equation (2.48) is transformed by substituting in for the currents, voltages, and back EMFs and then multiplying by $\boldsymbol{K}$ from the left. The mechanical equation (2.49) is transformed by substituting in for the currents and back EMFs. This results in

$$\boldsymbol{L}_{\alpha\beta\gamma}\frac{\mathrm{d}\boldsymbol{i}_{\alpha\beta\gamma}}{\mathrm{d}t} = -R_{\mathrm{s}}\boldsymbol{i}_{\alpha\beta\gamma} - \omega\boldsymbol{L}'_{\alpha\beta\gamma}\boldsymbol{i}_{\alpha\beta\gamma} - \boldsymbol{e}_{\alpha\beta\gamma} + \boldsymbol{v}_{\alpha\beta\gamma}, \tag{2.57}$$

$$J\frac{\mathrm{d}\omega}{\mathrm{d}t} = \frac{1}{2}\boldsymbol{i}_{\alpha\beta\gamma}^{\mathrm{T}}\boldsymbol{K}^{-\mathrm{T}}\boldsymbol{K}^{-1}\boldsymbol{L}'_{\alpha\beta\gamma}\boldsymbol{i}_{\alpha\beta\gamma} + \frac{1}{\omega}\boldsymbol{i}_{\alpha\beta\gamma}^{\mathrm{T}}\boldsymbol{K}^{-\mathrm{T}}\boldsymbol{K}^{-1}\boldsymbol{e}_{\alpha\beta\gamma} - B\omega + \tau_{\mathrm{cog}} + \tau_{\mathrm{ex}}, \tag{2.58}$$

$$\frac{\mathrm{d}\theta}{\mathrm{d}t} = \omega, \tag{2.59}$$

where

$$\boldsymbol{L}_{\alpha\beta\gamma} = \boldsymbol{K}\boldsymbol{L}_{\mathrm{sal}}\boldsymbol{K}^{-1}, \tag{2.60}$$

$$\boldsymbol{L}'_{\alpha\beta\gamma} = \frac{\partial \boldsymbol{L}_{\alpha\beta\gamma}}{\partial\theta}. \tag{2.61}$$

As the current i_γ is always zero, it is not associated with any energy transfer and the corresponding equation can be dropped. For this reason, one can use reduced Clarke transformation

$$\boldsymbol{i}_{\alpha\beta} = \begin{bmatrix} i_\alpha & i_\beta \end{bmatrix}^{\mathrm{T}} = \tilde{\boldsymbol{K}}\boldsymbol{i}_{\mathrm{abc}}, \tag{2.62}$$

$$\boldsymbol{v}_{\alpha\beta} = \begin{bmatrix} v_\alpha & v_\beta \end{bmatrix}^{\mathrm{T}} = \tilde{\boldsymbol{K}}\boldsymbol{v}_{\mathrm{abc}}, \tag{2.63}$$

$$\boldsymbol{e}_{\alpha\beta} = \begin{bmatrix} e_\alpha & e_\beta \end{bmatrix}^{\mathrm{T}} = \tilde{\boldsymbol{K}}\boldsymbol{e}_{\mathrm{abc}}, \tag{2.64}$$

where

$$\tilde{\boldsymbol{K}} = \frac{2}{3}\begin{bmatrix} 1 & -\frac{1}{2} & -\frac{1}{2} \\ 0 & \frac{\sqrt{3}}{2} & -\frac{\sqrt{3}}{2} \end{bmatrix}. \tag{2.65}$$

The model is then written as

$$\boldsymbol{L}_{\alpha\beta}\frac{\mathrm{d}\boldsymbol{i}_{\alpha\beta}}{\mathrm{d}t} = -R_{\mathrm{s}}\boldsymbol{i}_{\alpha\beta} - \omega\boldsymbol{L}'_{\alpha\beta}\boldsymbol{i}_{\alpha\beta} - \boldsymbol{e}_{\alpha\beta} + \boldsymbol{v}_{\alpha\beta}, \tag{2.66}$$

$$J\frac{\mathrm{d}\omega}{\mathrm{d}t} = \frac{3}{4}\boldsymbol{i}_{\alpha\beta}^{\mathrm{T}}\boldsymbol{L}'_{\alpha\beta}\boldsymbol{i}_{\alpha\beta} + \frac{3}{2\omega}\boldsymbol{i}_{\alpha\beta}^{\mathrm{T}}\boldsymbol{e}_{\alpha\beta} - B\omega + \tau_{\mathrm{cog}} + \tau_{\mathrm{ex}}, \tag{2.67}$$

$$\frac{\mathrm{d}\theta}{\mathrm{d}t} = \omega, \tag{2.68}$$

where $\boldsymbol{L}_{\alpha\beta}$ and $\boldsymbol{L}'_{\alpha\beta}$ are obtained from $\boldsymbol{L}_{\alpha\beta\gamma}$ and $\boldsymbol{L}'_{\alpha\beta\gamma}$ by taking only the first two columns and the first two rows. Inspecting

$$\boldsymbol{L}_{\alpha\beta} = \begin{bmatrix} L_{\mathrm{s}} + M_{\mathrm{s}} & 0 \\ 0 & L_{\mathrm{s}} + M_{\mathrm{s}} \end{bmatrix} + \frac{3}{2}L_{\mathrm{g}}\begin{bmatrix} \cos(2n_{\mathrm{pp}}\theta) & \sin(2n_{\mathrm{pp}}\theta) \\ \sin(2n_{\mathrm{pp}}\theta) & -\cos(2n_{\mathrm{pp}}\theta) \end{bmatrix}, \tag{2.69}$$

$$\boldsymbol{L}'_{\alpha\beta} = 3n_{\mathrm{pp}}L_{\mathrm{g}}\begin{bmatrix} -\sin(2n_{\mathrm{pp}}\theta) & \cos(2n_{\mathrm{pp}}\theta) \\ \cos(2n_{\mathrm{pp}}\theta) & \sin(2n_{\mathrm{pp}}\theta) \end{bmatrix}, \tag{2.70}$$

$$\boldsymbol{e}_{\alpha\beta} = -n_{\mathrm{pp}}\omega\,\Psi_{\mathrm{m}}\begin{bmatrix} \sin(n_{\mathrm{pp}}\theta) & -\cos(n_{\mathrm{pp}}\theta) \end{bmatrix}^{\mathrm{T}} \tag{2.71}$$

gives an insight into the transformed model. The model in $\alpha\beta$ variables is very similar to the model of two-phase PMSM with the two phases orthogonal to each other and magnetic

axis of phase α is aligned with magnetic axis of phase A. Phase β is rotated in space by +90 degrees from phase α. The difference is in the electromagnetic torque, which greater by a factor of 3/2 due to the fact that Clark transformation is not unitary and it does not preserve the magnitude of the transformed vectors.

The αβ variables are two differential modes of the abc variables and it is possible to obtain the transformed voltages by applying the Clarke transformation directly to the source voltages

$$\boldsymbol{v}_{\alpha\beta} = \tilde{\boldsymbol{K}} \begin{bmatrix} v_{\mathrm{as}} & v_{\mathrm{bs}} & v_{\mathrm{cs}} \end{bmatrix}^{\mathrm{T}}. \tag{2.72}$$

Further notes on the Clarke transformation are given in appendix A.

2.4 Transformation to DQ Variables

The model is further simplified by expressing αβγ variables in a rotating reference frame fixed to the rotor. In the resulting model, the dependence on the rotor angle is eliminated. This is done using Park transformation

$$\boldsymbol{i}_{\mathrm{dqz}} = \begin{bmatrix} i_{\mathrm{d}} & i_{\mathrm{q}} & i_{\mathrm{z}} \end{bmatrix}^{\mathrm{T}} = \boldsymbol{R}_{\mathrm{z}}\left(n_{\mathrm{pp}}\theta\right) \boldsymbol{i}_{\alpha\beta\gamma}, \tag{2.73}$$

$$\boldsymbol{v}_{\mathrm{dqz}} = \begin{bmatrix} v_{\mathrm{d}} & v_{\mathrm{q}} & v_{\mathrm{z}} \end{bmatrix}^{\mathrm{T}} = \boldsymbol{R}_{\mathrm{z}}\left(n_{\mathrm{pp}}\theta\right) \boldsymbol{v}_{\alpha\beta\gamma}, \tag{2.74}$$

$$\boldsymbol{e}_{\mathrm{dqz}} = \begin{bmatrix} e_{\mathrm{d}} & e_{\mathrm{q}} & e_{\mathrm{z}} \end{bmatrix}^{\mathrm{T}} = \boldsymbol{R}_{\mathrm{z}}\left(n_{\mathrm{pp}}\theta\right) \boldsymbol{e}_{\alpha\beta\gamma}, \tag{2.75}$$

where the rotation matrix is

$$\boldsymbol{R}_{\mathrm{z}}\left(\varphi\right) = \begin{bmatrix} \cos\left(\varphi\right) & \sin\left(\varphi\right) & 0 \\ -\sin\left(\varphi\right) & \cos\left(\varphi\right) & 0 \\ 0 & 0 & 1 \end{bmatrix}. \tag{2.76}$$

The first component of the transformed variables is called direct component, the second is called quadrature component, and the third is called zero component.

The voltage equation (2.57) is transformed by substituting in for the currents, voltages, and back EMFs and then multiplying by $\boldsymbol{R}_{\mathrm{z}}\left(n_{\mathrm{pp}}\theta\right)$ from the left. The mechanical equation (2.58) is transformed by substituting in for the currents and back EMFs. This results in

$$\boldsymbol{L}_{\mathrm{dqz}} \frac{\mathrm{d}\boldsymbol{i}_{\mathrm{dqz}}}{\mathrm{d}t} = -R_{\mathrm{s}}\boldsymbol{i}_{\mathrm{dqz}} - \omega\tilde{\tilde{\boldsymbol{L}}}_{\mathrm{dqz}}\boldsymbol{i}_{\mathrm{dqz}} - \boldsymbol{e}_{\mathrm{dqz}} + \boldsymbol{v}_{\mathrm{dqz}}, \tag{2.77}$$

$$J\frac{\mathrm{d}\omega}{\mathrm{d}t} = \frac{1}{2}\boldsymbol{i}_{\mathrm{dqz}}^{\mathrm{T}}\boldsymbol{K}^{-\mathrm{T}}\boldsymbol{K}^{-1}\tilde{\boldsymbol{L}}_{\mathrm{dqz}}\boldsymbol{i}_{\mathrm{dqz}} + \frac{1}{\omega}\boldsymbol{i}_{\mathrm{dqz}}^{\mathrm{T}}\boldsymbol{K}^{-\mathrm{T}}\boldsymbol{K}^{-1}\boldsymbol{e}_{\mathrm{dqz}} - B\omega + \tau_{\mathrm{cog}} + \tau_{\mathrm{ex}}, \tag{2.78}$$

$$\frac{\mathrm{d}\theta}{\mathrm{d}t} = \omega, \tag{2.79}$$

where

$$\boldsymbol{L}_{\mathrm{dqz}} = \boldsymbol{R}_{\mathrm{z}}\boldsymbol{L}_{\alpha\beta\gamma}\boldsymbol{R}_{\mathrm{z}}^{-1}, \tag{2.80}$$

$$\tilde{\boldsymbol{L}}_{\mathrm{dqz}} = \boldsymbol{R}_{\mathrm{z}}\boldsymbol{L}'_{\alpha\beta\gamma}\boldsymbol{R}_{\mathrm{z}}^{-1}, \tag{2.81}$$

$$\tilde{\tilde{\boldsymbol{L}}}_{\mathrm{dqz}} = \tilde{\boldsymbol{L}}_{\mathrm{dqz}} + \boldsymbol{R}_{\mathrm{z}}\boldsymbol{L}_{\alpha\beta\gamma}\frac{\partial \boldsymbol{R}_{\mathrm{z}}^{-1}}{\partial\theta}. \tag{2.82}$$

As the third component of the transformed variables is zero and the equation for i_{z} can be dropped, the transformation can be done for the direct and quadrature components only

$$\boldsymbol{i}_{\mathrm{dq}} = \begin{bmatrix} i_{\mathrm{d}} & i_{\mathrm{q}} \end{bmatrix}^{\mathrm{T}} = \tilde{\boldsymbol{R}}_{\mathrm{z}}\left(n_{\mathrm{pp}}\theta\right)\boldsymbol{i}_{\alpha\beta}, \tag{2.83}$$

$$\boldsymbol{v}_{\mathrm{dq}} = \begin{bmatrix} v_{\mathrm{d}} & v_{\mathrm{q}} \end{bmatrix}^{\mathrm{T}} = \tilde{\boldsymbol{R}}_{\mathrm{z}}\left(n_{\mathrm{pp}}\theta\right)\boldsymbol{v}_{\alpha\beta}, \tag{2.84}$$

$$\boldsymbol{e}_{\mathrm{dq}} = \begin{bmatrix} e_{\mathrm{d}} & e_{\mathrm{q}} \end{bmatrix}^{\mathrm{T}} = \tilde{\boldsymbol{R}}_{\mathrm{z}}\left(n_{\mathrm{pp}}\theta\right)\boldsymbol{e}_{\alpha\beta}, \tag{2.85}$$

where the rotation matrix is

$$\tilde{\boldsymbol{R}}_{\mathrm{z}}\left(\varphi\right) = \begin{bmatrix} \cos\left(\varphi\right) & \sin\left(\varphi\right) \\ -\sin\left(\varphi\right) & \cos\left(\varphi\right) \end{bmatrix}. \tag{2.86}$$

The model is then written as

$$\boldsymbol{L}_{\mathrm{dq}}\frac{\mathrm{d}\boldsymbol{i}_{\mathrm{dq}}}{\mathrm{d}t} = -R_{\mathrm{s}}\boldsymbol{i}_{\mathrm{dq}} - \omega\tilde{\tilde{\boldsymbol{L}}}_{\mathrm{dq}}\boldsymbol{i}_{\mathrm{dq}} - \boldsymbol{e}_{\mathrm{dq}} + \boldsymbol{v}_{\mathrm{dq}}, \tag{2.87}$$

$$J\frac{\mathrm{d}\omega}{\mathrm{d}t} = \frac{3}{4}\boldsymbol{i}_{\mathrm{dq}}^{\mathrm{T}}\tilde{\boldsymbol{L}}_{\mathrm{dq}}\boldsymbol{i}_{\mathrm{dq}} + \frac{3}{2\omega}\boldsymbol{i}_{\mathrm{dq}}^{\mathrm{T}}\boldsymbol{e}_{\mathrm{dq}} - B\omega + \tau_{\mathrm{cog}} + \tau_{\mathrm{ex}}, \tag{2.88}$$

$$\frac{\mathrm{d}\theta}{\mathrm{d}t} = \omega, \tag{2.89}$$

where

$$\boldsymbol{L}_{\mathrm{dq}} = \begin{bmatrix} L_{\mathrm{s}} + M_{\mathrm{s}} + \frac{3}{2}L_{\mathrm{g}} & 0 \\ 0 & L_{\mathrm{s}} + M_{\mathrm{s}} - \frac{3}{2}L_{\mathrm{g}} \end{bmatrix}, \tag{2.90}$$

$$\tilde{\boldsymbol{L}}_{\mathrm{dq}} = 3n_{\mathrm{pp}}\begin{bmatrix} 0 & L_{\mathrm{g}} \\ L_{\mathrm{g}} & 0 \end{bmatrix}, \tag{2.91}$$

$$\tilde{\tilde{\boldsymbol{L}}}_{\mathrm{dq}} = n_{\mathrm{pp}}\begin{bmatrix} 0 & -\left(L_{\mathrm{s}} + M_{\mathrm{s}} - \frac{3}{2}L_{\mathrm{g}}\right) \\ L_{\mathrm{s}} + M_{\mathrm{s}} + \frac{3}{2}L_{\mathrm{g}} & 0 \end{bmatrix} \tag{2.92}$$

$$\boldsymbol{e}_{\mathrm{dq}} = n_{\mathrm{pp}}\omega\,\Psi_{\mathrm{m}}\begin{bmatrix} 0 & 1 \end{bmatrix}^{\mathrm{T}}. \tag{2.93}$$

The direct and quadrature inductances are defined as

$$L_\mathrm{d} = L_\mathrm{s} + M_\mathrm{s} + \frac{3}{2}L_\mathrm{g}, \tag{2.94}$$

$$L_\mathrm{q} = L_\mathrm{s} + M_\mathrm{s} - \frac{3}{2}L_\mathrm{g}. \tag{2.95}$$

The back-EMF constant is defined as

$$K_\mathrm{b} = n_\mathrm{pp}\,\Psi_\mathrm{m}. \tag{2.96}$$

The DQ model of PMSM is then expressed in scalar form as

$$L_\mathrm{d}\frac{\mathrm{d}i_\mathrm{d}}{\mathrm{d}t} = -R_\mathrm{s}i_\mathrm{d} + n_\mathrm{pp}\omega L_\mathrm{q}i_\mathrm{q} + v_\mathrm{d}, \tag{2.97}$$

$$L_\mathrm{q}\frac{\mathrm{d}i_\mathrm{q}}{\mathrm{d}t} = -R_\mathrm{s}i_\mathrm{q} - n_\mathrm{pp}\omega L_\mathrm{d}i_\mathrm{d} - K_\mathrm{b}\omega + v_\mathrm{q}, \tag{2.98}$$

$$J\frac{\mathrm{d}\omega}{\mathrm{d}t} = \frac{3}{2}n_\mathrm{pp}i_\mathrm{d}i_\mathrm{q}(L_\mathrm{d} - L_\mathrm{q}) + \frac{3}{2}K_\mathrm{b}i_\mathrm{q} - B\omega + \tau_\mathrm{cog} + \tau_\mathrm{ex}, \tag{2.99}$$

$$\frac{\mathrm{d}\theta}{\mathrm{d}t} = \omega. \tag{2.100}$$

From this model, model of PMSM with uniform air gap is obtained by setting $L_\mathrm{d} = L_\mathrm{q}$ and $\tau_\mathrm{cog} = 0$. The main component of the electromagnetic torque is the synchronous torque $3K_\mathrm{b}i_\mathrm{q}/2$ and the reluctance torque $3n_\mathrm{pp}i_\mathrm{d}i_\mathrm{q}(L_\mathrm{d} - L_\mathrm{q})/2$ is usually significantly smaller. In other words, the electromagnetic torque is primarily produced by the quadrature current i_q alone. The direct current i_d creates magnetic field aligned with the rotor magnetic field and does not produce significant torque. At low speeds, the direct current is usually commanded to zero. At high speeds, it is commanded to negative values to weaken the rotor magnetic field in order to decrease the voltage induced in the quadrature phase.

In steady state with constant rotor speed and sinusoidal phase currents given in (2.44), the direct current is zero and the quadrature current is the amplitude of the phase currents. More generally, if the steady-state currents are as given in (2.46), then

$$i_\mathrm{d} = I_\mathrm{m}\sin(\phi), \tag{2.101}$$

$$i_\mathrm{q} = I_\mathrm{m}\cos(\phi). \tag{2.102}$$

2.5 Linearized Model

For control purposes, the DQ model of PMSM is linearized into the following standard state-space form

$$\dot{\boldsymbol{x}} = \boldsymbol{A}_\mathrm{c}\boldsymbol{x} + \boldsymbol{B}_\mathrm{c}\boldsymbol{u}, \tag{2.103}$$

$$\boldsymbol{y} = \boldsymbol{C}_\mathrm{c}\boldsymbol{x} + \boldsymbol{D}_\mathrm{c}\boldsymbol{u}, \tag{2.104}$$

where the state vector and input vector are

$$\boldsymbol{x} = \begin{bmatrix} i_\mathrm{d} & i_\mathrm{q} & \omega & \theta \end{bmatrix}^\mathrm{T}, \tag{2.105}$$

$$\boldsymbol{u} = \begin{bmatrix} v_\mathrm{d} & v_\mathrm{q} \end{bmatrix}^\mathrm{T}. \tag{2.106}$$

The cogging torque and the external torque are not considered in this model. The linear DQ model is obtained by making a two assumptions and approximations, which simplify the nonlinear model into a linear one. Firstly, the reluctance torque is neglected as it is usually small compared to the synchronous torque. Secondly, it is assumed that ω does not change too much during controller sampling period, or over the prediction horizon in case of MPC. This justifies one to consider ω a constant parameter in the nonlinear terms $n_\mathrm{pp}\omega L_\mathrm{q} i_\mathrm{q}$ and $n_\mathrm{pp}\omega L_\mathrm{d} i_\mathrm{d}$. This gives linear time-varying model

$$\boldsymbol{A}_\mathrm{c} = \begin{bmatrix} -\frac{R_\mathrm{s}}{L_\mathrm{d}} & n_\mathrm{pp}\omega\frac{L_\mathrm{q}}{L_\mathrm{d}} & 0 & 0 \\ -n_\mathrm{pp}\omega\frac{L_\mathrm{d}}{L_\mathrm{q}} & -\frac{R_\mathrm{s}}{L_\mathrm{q}} & -\frac{K_\mathrm{b}}{L_\mathrm{q}} & 0 \\ 0 & \frac{3}{2}\frac{K_\mathrm{b}}{J} & -\frac{B}{J} & 0 \\ 0 & 0 & 1 & 0 \end{bmatrix}, \boldsymbol{B}_\mathrm{c} = \begin{bmatrix} \frac{1}{L_\mathrm{d}} & 0 \\ 0 & \frac{1}{L_\mathrm{q}} \\ 0 & 0 \\ 0 & 0 \end{bmatrix} \tag{2.107}$$

parametrized by ω. Matrix $\boldsymbol{D}_\mathrm{c} = \boldsymbol{0}$ is zero matrix and $\boldsymbol{C}_\mathrm{c}$ is chosen based on the control objective. Such linearized model was also used in [13].

2.6 Discretization

Discrete-time linear model of PMSM with sampling period T_s

$$\boldsymbol{x}_{k+1} = \boldsymbol{A}_\mathrm{d}\boldsymbol{x}_k + \boldsymbol{B}_\mathrm{d}\boldsymbol{u}_k, \tag{2.108}$$

$$\boldsymbol{y}_k = \boldsymbol{C}_\mathrm{d}\boldsymbol{x}_k + \boldsymbol{D}_\mathrm{d}\boldsymbol{u}_k \tag{2.109}$$

is obtained from the continuous-time model assuming constant inputs over the sampling period, which results in

$$\boldsymbol{A}_\mathrm{d} = e^{T_\mathrm{s}\boldsymbol{A}_\mathrm{c}}, \tag{2.110}$$

$$\boldsymbol{B}_\mathrm{d} = \left(\int_{\tau=0}^{\tau=T_\mathrm{s}} e^{\tau\boldsymbol{A}_\mathrm{c}} \mathrm{d}\tau \right) \boldsymbol{B}_\mathrm{c}, \tag{2.111}$$

$$\boldsymbol{C}_\mathrm{d} = \boldsymbol{C}_\mathrm{c}, \tag{2.112}$$

$$\boldsymbol{D}_\mathrm{d} = \boldsymbol{D}_\mathrm{c}. \tag{2.113}$$

When the discrete-time state-space matrices are to be computed online within a limited amount of time, Euler approximation

$$\boldsymbol{A}_\mathrm{d} \approx \boldsymbol{I} + T_\mathrm{s}\boldsymbol{A}_\mathrm{c}, \tag{2.114}$$

$$\boldsymbol{B}_\mathrm{d} \approx T_\mathrm{s}\boldsymbol{B}_\mathrm{c} \tag{2.115}$$

can be used.

2.7 Model Parameters

Usually, datasheets provide only line-to-line inductance $L_\text{line-line}$, line-to-line resistance $R_\text{line-line}$, and torque constant K_t or line-to-line back-EMF constant $K_\mathrm{b}^\text{line-line}$. The relationships between the datasheet parameters and the model parameters are presented in [6]. However, the DQ model in [6] is derived using different Clarke transformation and different definition of the back-EMF constant than the one used here. For the sake of completeness and to make things clear, the same procedure as in [6] is adapted for the parameters used here.

Now, star-connected PMSM with uniform air gap is assumed. The direct and quadrature inductances are equal $L = L_\mathrm{d} = L_\mathrm{q}$. The line-to-line inductance and resistance are measured with locked rotor by applying voltage between two terminal, e.g. A and B, and the third terminal is left unconnected. Thus, $\omega = 0$, $i_\mathrm{c} = 0$, and $i_\mathrm{b} = -i_\mathrm{a}$. The equations for i_a and i_b are obtained from (2.48) by substituting in for ω are

$$L_\mathrm{s}\frac{\mathrm{d}i_\mathrm{a}}{\mathrm{d}t} - M_\mathrm{s}\frac{\mathrm{d}i_\mathrm{b}}{\mathrm{d}t} = -R_\mathrm{s}i_\mathrm{a} + v_\mathrm{a}, \tag{2.116}$$

$$-M_\mathrm{s}\frac{\mathrm{d}i_\mathrm{a}}{\mathrm{d}t} + L_\mathrm{s}\frac{\mathrm{d}i_\mathrm{b}}{\mathrm{d}t} = -R_\mathrm{s}i_\mathrm{b} + v_\mathrm{b}. \tag{2.117}$$

Substituting in $i_\mathrm{b} = -i_\mathrm{a}$ and substracting the second equation from the first one gives

$$2(L_\mathrm{s} + M_\mathrm{s})\frac{\mathrm{d}i_\mathrm{a}}{\mathrm{d}t} = -2R_\mathrm{s} + (v_\mathrm{a} - v_\mathrm{b}). \tag{2.118}$$

Therefore, the line-to-line inductance and resistance are

$$L_\text{line-line} = 2(L_\mathrm{s} + M_\mathrm{s}), \tag{2.119}$$

$$R_\text{line-line} = 2R_\mathrm{s}. \tag{2.120}$$

Comparing the line-to-line inductance with the definition of L_d in (2.94) and definition of L_q in (2.95) gives

$$L = L_\mathrm{d} = L_\mathrm{q} = \frac{1}{2}L_\text{line-line}, \tag{2.121}$$

$$R_\mathrm{s} = \frac{1}{2}R_\text{line-line}. \tag{2.122}$$

The line-to-line back-EMF constant is measured by leaving all motor terminals unconnected and rotating the rotor at constant speed using another motor. Thus, $i_\mathrm{a} = i_\mathrm{b} = i_\mathrm{c} = 0$. The induced voltage is measured between two terminals, e.g. B and C. The equations for v_b and v_c are obtained from (2.48) by substituting in for the currents

$$v_\mathrm{b} = n_\mathrm{pp}\omega\,\Psi_\mathrm{m}\sin\left(n_\mathrm{pp}\theta - \frac{2\pi}{3}\right), \tag{2.123}$$

$$v_\mathrm{c} = n_\mathrm{pp}\omega\,\Psi_\mathrm{m}\sin\left(n_\mathrm{pp}\theta + \frac{2\pi}{3}\right). \tag{2.124}$$

Substracting the second equation from the first one and rearranging gives

$$\frac{v_\mathrm{b} - v_\mathrm{b}}{\omega} = \sqrt{3}n_\mathrm{pp}\,\Psi_\mathrm{m}\cos\left(n_\mathrm{pp}\theta\right). \tag{2.125}$$

Therefore, the line-to-line back-EMF constant relating the amplitude of the induced line-to-line voltage to the rotor speed is

$$K_\mathrm{b}^\text{line-line} = \sqrt{3}n_\mathrm{pp}\,\Psi_\mathrm{m}. \tag{2.126}$$

Comparing with the definition of K_b in (2.96) gives

$$K_\mathrm{b} = \frac{1}{\sqrt{3}}K_\mathrm{b}^\text{line-line}. \tag{2.127}$$

The torque constant relates the generated electromagnetic torque to the root mean square (RMS) value of the source currents in steady state when the currents are sinusoidal and synchronized with the rotor as in (2.44). Such currents result in constant torque given in (2.45). Thus, the torque constant is

$$K_\mathrm{t} = \sqrt{2}\frac{3}{2}n_\mathrm{pp}\,\Psi_\mathrm{m} \tag{2.128}$$

and

$$K_\mathrm{b} = \frac{1}{\sqrt{2}}\frac{2}{3}K_\mathrm{t}. \tag{2.129}$$

Both $K_\mathrm{b}^\text{line-line}$ and K_b have units of $\mathrm{V_{(peak)}/(rad/s)} = \mathrm{N\,m/A_{(peak)}}$ whereas K_t has unit of $\mathrm{V_{(rms)}/(rad/s)} = \mathrm{N\,m/A_{(rms)}}$. However, some datasheets give the torque constant using the peak current and/or the line-to-line back-EMF constant using the RMS voltage. When motor saliency is to be considered, one usually has to identify the inductances L_d and L_q as they are not usually provided by the manufacturer.

Similar but slightly modified steps can be taken for delta-connected PMSM to find the relationships between the datasheet parameters and the parameters used here. Another approach is to treat the motor as star-connected and the star-equivalent parameters are obtained in the same way as for an actual star-connected PMSM. This is justified in appendix A.

The control algorithms inspected in this thesis were evaluated on PMSM BLWR233D-36V-4000 by Anaheim Automation. (According to the manufacturer it is BLDC motor, however, according to the terminology used here, it is rather PMSM.) The motor is delta-connected but it was treated as star-connected using star-equivalent parameters. The parameters given in datasheet [14] are in tab. 2.1. The motor is designed such that it can continuously operate at rated conditions without overheating. At the rated conditions, the motor is controlled such that it rotates at the rated speed with an external load torque equal to the rated torque, $\tau_{\mathrm{ex}} = -0.22\,\mathrm{N\,m}$. The rated current is the steady-state RMS value of the source currents running to the motor terminals. The generated electromagnetic torque equals the rated current times the torque constant and is approximately equal to the rated torque. There is, however, a small component of the electromagnetic torque that compensates for the friction. As the coefficient of viscous friction is not given in the datasheet, one might try to estimate B from the precision of the rated values assigning the difference between the electromagnetic torque and the load torque to the friction torque. This would, however, provide very inaccurate and uncertain value and one should rather identify B experimentally. The rated voltage is recommended inverter DC-bus voltage v_{dc}.

For the control design, experimentally identified star-equivalent parameters were used. The identification method used to obtain these parameters was similar to the one in [15]. The identified parameters and parameters derived from the datasheet are in tab. 2.2.

2.8 Constraints

PMSM manufacturers usually state two constraints on the currents supplied to the motor terminals. The first one is the rated current, which is the maximum current at which the motor can operate continuously without overheating. The second one is the peak current, which can be supplied to the motor terminals for short period of time. Thus, the current can be increased above the rated current up to the peak current for certain amount of time and then it must not exceed the rated current for some other amount of time to prevent overheating. To simplify the control task, single hard constraint is imposed on the phase currents using the fact that the phase currents are equal to the source currents when star-connected PMSM model is used. As the motor is to be operated both at high speeds with sinusoidal phase curents and at speeds close to zero with almost constant currents, the RMS value of the rated current is used as the limit on the instantaneous values of the phase currents. Although this conservative choice reduces the maximum admissible torque at the rated speed, it enables simple formulation of the constraints

$$|i_{\mathrm{a}}| \leq I_{\max}, \tag{2.130}$$

$$|i_{\mathrm{b}}| \leq I_{\max}, \tag{2.131}$$

$$|i_{\mathrm{c}}| \leq I_{\max}, \tag{2.132}$$

$$I_{\max} = 3.67\,\mathrm{A}. \tag{2.133}$$

Parameter	Given value	Converted to SI
Number of poles	4	4
Rated voltage	36 V	36 V
Rated speed	4000 RPM	$418.9\,\mathrm{rad\,s^{-1}}$
Rated power	92 W	92 W
Rated torque	31.2 ozf in	0.22 N m
Peak torque	93.5 ozf in	0.66 N m
Rated current	$3.67\,\mathrm{A_{(rms)}}$	$3.67\,\mathrm{A_{(rms)}}$
Line-to-line resistance	0.64 Ω	0.64 Ω
Line-to-line inductance	2.1 mH	2.1 mH
Torque constant	$8.50\,\mathrm{ozf\,in\,A_{(rms)}^{-1}}$	$0.06\,\mathrm{N\,m\,A_{(rms)}^{-1}}$
Rotor inertia	$0.00169\,\mathrm{ozf\,in\,s^2}$	$1.19 \times 10^{-5}\,\mathrm{kg\,m^2}$

Table 2.1: Parameters given in datasheet for BLWR233D-36V-4000 motor.

Parameter	Symbol	Identified	From datasheet	Unit
Number of pole pairs	n_{pp}	2	2	1
Phase resistance	R_{s}	0.45	0.32	Ω
Direct inductance	L_{d}	0.8	1.05	mH
Quadrature inductance	L_{q}	0.9	1.05	mH
Back-EMF constant	K_{b}	0.23	0.028	$\mathrm{V_{(peak)}/(rad/s)}$
Rotor inertia	J	2.8×10^{-5}	1.19×10^{-5}	$\mathrm{kg\,m^2}$
Friction coefficient	B	1.3×10^{-5}	–	Nm/(rad/s)

Table 2.2: Star-equivalent parameters identified experimentally and derived from datasheet.

The Clarke transformation translates these constraints to

$$|i_\alpha| \;\leq\; I_{\max}, \tag{2.134}$$

$$\left|i_\alpha + \sqrt{3} i_\beta\right| \;\leq\; 2I_{\max}, \tag{2.135}$$

$$\left|i_\alpha - \sqrt{3} i_\beta\right| \;\leq\; 2I_{\max}, \tag{2.136}$$

which is area bounded by a hexagon as shown in fig. 2.6(a). In order to transform this feasible region to the rotating reference frame it is approximated by inscribed disk

$$i_\alpha^2 + i_\beta^2 \;\leq\; I_{\max}^2. \tag{2.137}$$

The disk remains unchanged when Park transformation is applied and it is written in the DQ variables as

$$i_{\mathrm{d}}^2 + i_{\mathrm{q}}^2 \;\leq\; I_{\max}^2. \tag{2.138}$$

This nonlinear constraint is further approximated by set of linear constraints. Specifically, octagon is used as the approximated feasible region in a similar way as in [2]. The octagon is in fig. 2.6(c) and is described by

$$\boldsymbol{P}_x \boldsymbol{x} \;\leq\; \boldsymbol{p}_x, \tag{2.139}$$

where

$$\boldsymbol{P}_x \;=\; \begin{bmatrix} +1 & +\sqrt{2}-1 & 0 & 0 \\ +1 & -\sqrt{2}+1 & 0 & 0 \\ -1 & +\sqrt{2}-1 & 0 & 0 \\ -1 & -\sqrt{2}+1 & 0 & 0 \\ +\sqrt{2}-1 & +1 & 0 & 0 \\ +\sqrt{2}-1 & -1 & 0 & 0 \\ -\sqrt{2}+1 & +1 & 0 & 0 \\ -\sqrt{2}+1 & -1 & 0 & 0 \end{bmatrix}, \quad \boldsymbol{p}_x = \begin{bmatrix} I_{\max} \\ I_{\max} \\ I_{\max} \\ I_{\max} \\ I_{\max} \\ I_{\max} \\ I_{\max} \\ I_{\max} \end{bmatrix}. \tag{2.140}$$

In this thesis, no constraints are imposed on the other two state variables, the rotor velocity and position.

Assuming that the inverter always connects each phase to either $+v_{\mathrm{dc}}/2$ or $-v_{\mathrm{dc}}/2$ and that no phase is left unconnected, there are 8 possible voltage vectors that can be applied to the motor. When modulation stage is used, one can assume that each source voltage is a real value from interval $[-v_{\mathrm{dc}}/2, +v_{\mathrm{dc}}/2]$. Thus, constraints on the source voltages are

$$|v_{\mathrm{as}}| \;\leq\; \frac{1}{2} v_{\mathrm{dc}}, \tag{2.141}$$

$$|v_{\mathrm{bs}}| \;\leq\; \frac{1}{2} v_{\mathrm{dc}}, \tag{2.142}$$

$$|v_{\mathrm{cs}}| \;\leq\; \frac{1}{2} v_{\mathrm{dc}}, \tag{2.143}$$

where $v_{\mathrm{dc}} = 24\,\mathrm{V}$ was chosen instead of the rated voltage. These constraints are translated by the Clarke transformation using

$$\boldsymbol{v}_{\mathrm{abcs}} = \boldsymbol{K}^{-1} \boldsymbol{v}_{\alpha\beta\gamma} + \begin{bmatrix} v_{\mathrm{cms}} & v_{\mathrm{cms}} & v_{\mathrm{cms}} \end{bmatrix}^{\mathrm{T}}, \tag{2.144}$$

where the common-mode voltage v_{cms} is chosen arbitrarily. The constraint on the $\alpha\beta$ voltages

are

$$|v_\alpha + v_{\text{cms}}| \leq \frac{1}{2}v_{\text{dc}}, \tag{2.145}$$

$$\left|v_\alpha + \sqrt{3}v_\beta + 2v_{\text{cms}}\right| \leq v_{\text{dc}}, \tag{2.146}$$

$$\left|v_\alpha - \sqrt{3}v_\beta + 2v_{\text{cms}}\right| \leq v_{\text{dc}} \tag{2.147}$$

and the feasible region consists of all points $\boldsymbol{v}_{\alpha\beta}$ for which some v_{cms} exists such that these conditions are satisfied. The extra degree of freedom in form of v_{cms} enlarges the feasible region to

$$\left|v_\beta\right| \leq \frac{1}{\sqrt{3}}v_{\text{dc}}, \tag{2.148}$$

$$\left|v_\beta + \sqrt{3}v_\alpha\right| \leq \frac{2}{\sqrt{3}}v_{\text{dc}}, \tag{2.149}$$

$$\left|v_\beta - \sqrt{3}v_\alpha\right| \leq \frac{2}{\sqrt{3}}v_{\text{dc}}, \tag{2.150}$$

which is area bounded by a hexagon as shown in fig. 2.6(b). In order to transform this feasible region to the rotating reference frame it is approximated by inscribed disk

$$v_\alpha^2 + v_\beta^2 \leq V_{\text{max}}^2, \tag{2.151}$$

$$V_{\text{max}} = \frac{v_{\text{dc}}}{\sqrt{3}}. \tag{2.152}$$

The disk remains unchanged when Park transformation is applied and it is written in the DQ variables as

$$v_{\text{d}}^2 + v_{\text{q}}^2 \leq V_{\text{max}}^2. \tag{2.153}$$

This nonlinear constraint is again approximated by octagon

$$\boldsymbol{P}_u\boldsymbol{u} \leq \boldsymbol{p}_u, \tag{2.154}$$

where

$$\boldsymbol{P}_u = \begin{bmatrix} +1 & +\sqrt{2}-1 \\ +1 & -\sqrt{2}+1 \\ -1 & +\sqrt{2}-1 \\ -1 & -\sqrt{2}+1 \\ +\sqrt{2}-1 & +1 \\ +\sqrt{2}-1 & -1 \\ -\sqrt{2}+1 & +1 \\ -\sqrt{2}+1 & -1 \end{bmatrix}, \quad \boldsymbol{p}_u = \begin{bmatrix} V_{\text{max}} \\ V_{\text{max}} \\ V_{\text{max}} \\ V_{\text{max}} \\ V_{\text{max}} \\ V_{\text{max}} \\ V_{\text{max}} \\ V_{\text{max}} \end{bmatrix}. \tag{2.155}$$

The octagon is in fig. 2.6(d).

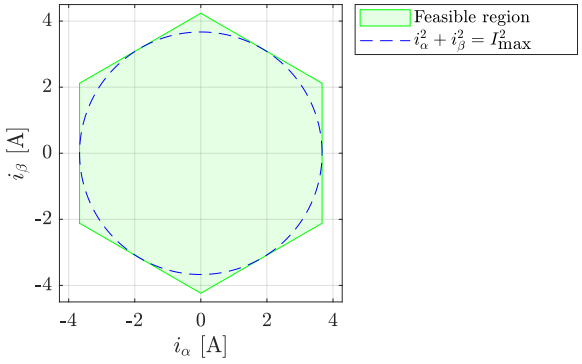

(a) Constraints on αβ currents.

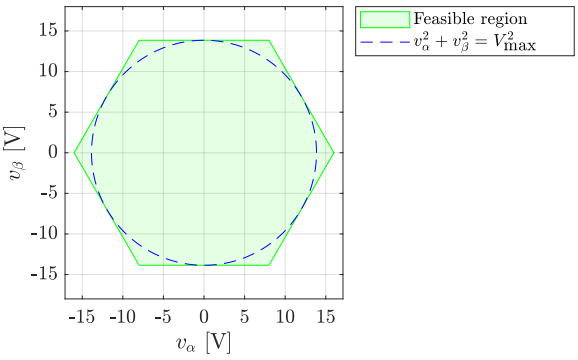

(b) Constraints on αβ voltages.

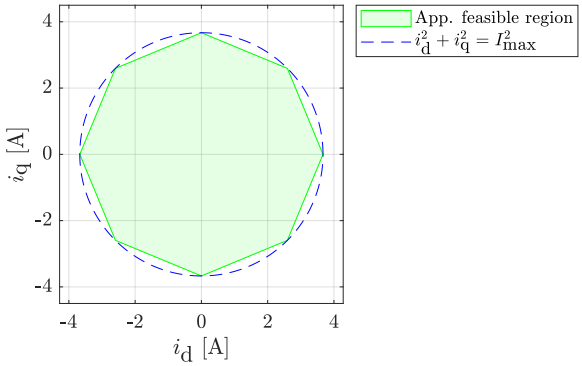

(c) Aprroximated constraints on DQ currents.

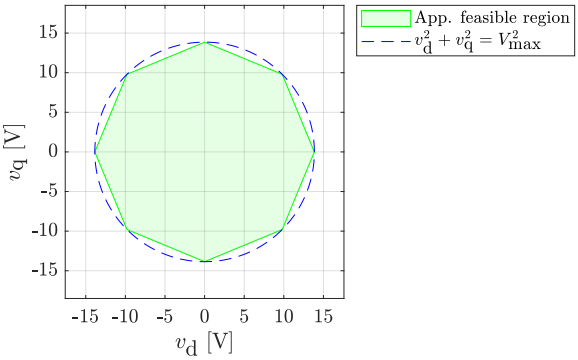

(d) Approximated constraints on DQ voltages.

Figure 2.6: Current and voltage constraints transformed to αβ variables (a) and (b), and approximated constraints in DQ variables (c) and (d).

Chapter 3

Control for PMSM

This chapter describes the examined control algorithms. Firstly, different controller structures are compared. Then, voltage modulation schemes are briefly discussed. Finally, three types of PMSM controllers are described: PI controller, CCS-MPC, and FCS-MPC. All of them are so called field oriented because they are formulated in the DQ variables, where each of the two DQ currents defines one components of the generated magnetic field. When reluctance torque is neglected, only quadrature current generates torque. Thus, control of electromagnetic torque is easily reformulated to control of the quadrature current.

The field-weakening operation is not considered here and the controllers are intended to operate at lower speeds. At low speeds, the maximum torque can be generated by commanding i_d to zero and i_q to the maximum possible value. There is a transition speed above which i_d should be commanded to negative values in order to achieve the maximum torque. For the used motor and inverter DC-bus voltage 24 V, the transition speed is around 4100 RPM (it would be around 6300 RPM for the rated voltage). Current references maximizing torque above the transition speed are given in [6]. The formulations of MPC used here are inherently capable of flux weakening to some extent by choosing small penalization of the deviation of the direct current from zero. On the other hand, small penalization enlarges the direct current and the power losses even at lower speeds. More subtle solutions choose the cost function and state vector differently and yield better results. Examples of such solutions are [16] and [17].

3.1 General Controller Structures

To control PMSM using the DQ model, the controller structure in fig. 3.1 is often used. The measured three-phase currents are transformed to the DQ currents. Based on the state variables $\boldsymbol{x}$ and the references $\boldsymbol{r}$, DQ voltages are computed and transformed to three-phase voltages. The common-mode can be adjusted or left zero. The voltages then modulate the switching signals to the inverter by means of PWM. The actual voltages applied to the motor are v_ai, v_bi, v_ci, and v_as, v_bs, v_cs are rather reference values. The structure is simpler for FCS-MPC. In that case, the control algorithm generates the switching signals directly and the inverse transformations and modulation stage are not present. Also, the sample rate should be higher than with modulation stage.

When rotor velocity or angle are to be controlled, single-loop or cascaded multi-loop structures in fig. 3.2 can be considered. The cascaded multi-loop comprises three nested controllers. The position controller G_3 generates reference for the velocity controller G_2,

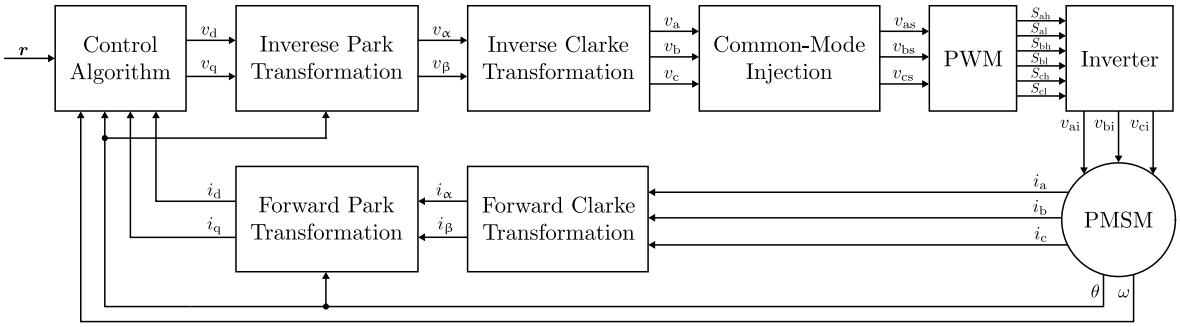

Figure 3.1: Typical structure of PMSM controller.

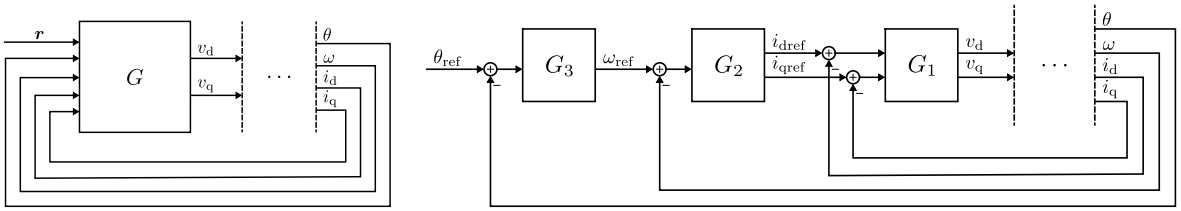

(a) Single-loop controller.

(b) Cascaded multi-loop controller.

Figure 3.2: Comparison of structures of single-loop and cascaded multi-loop controllers. (The three dots stand for the transformations, modulation stage, inverter, and motor.)

which generates references for the current controller G_1. Controller G_1 should have higher sample rate than G_2 and the current control loop should have faster dynamic response than the velocity control loop. Similarly, G_2 should have higher sample rate than G_3 and the velocity control loop should have faster dynamic response than the position control loop. This usually achievable for electric motors as the electrical time constants $\tau_d = L_d/R_s$ and $\tau_q = L_q/R_s$ are usually noticeably smaller than the mechanical time constant $\tau_m = J/B$. The single-loop structure, on the other hand, can take the whole dynamic model of PMSM into account and provide better performance, especially when the time constants are close to each other. However, significant difference in the time constants might be challenging for single-loop controllers.

3.2 Voltage modulation

Carrier-based digital PWM is commonly used by digital controllers. There are three variants, trailing-edge, leading-edge, and symmetrical PWM, which are described in [18]. Three single-phase PWM modulators can be used for control of PMSMs but there is another modulation scheme designed specifically for three-phase motors called space-vector modulation (SVM). It replaces the inverse Clarke transformation, common-mode injection, and PWM, and expresses $\boldsymbol{v}_{\alpha\beta}$ in terms of the eight achievable voltage vectors $\boldsymbol{v}_{\alpha\beta 0}$, $\boldsymbol{v}_{\alpha\beta 1}$, …, $\boldsymbol{v}_{\alpha\beta 7}$ the inverter can apply to the motor. The eigth achievable vectors are in tab. 3.1 and as shown in fig. 3.3,

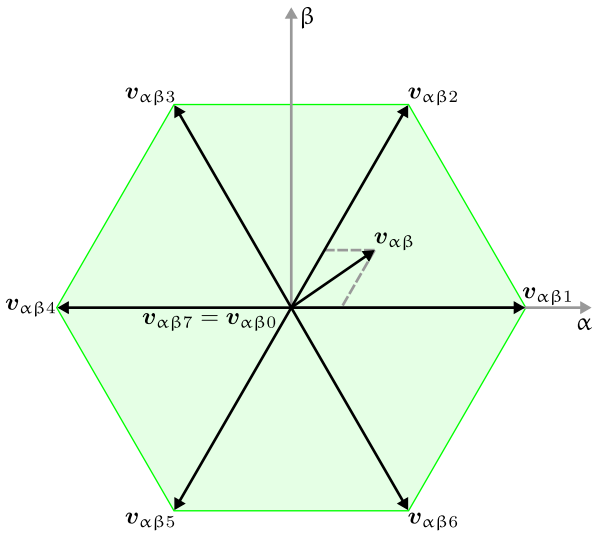

Figure 3.3: SVM expresses vector $\boldsymbol{v}_{\alpha\beta}$ as a linear combination of the adjacent achievable vectors and zero vectors.

vectors $\boldsymbol{v}_{\alpha\beta1}, \ldots, \boldsymbol{v}_{\alpha\beta6}$ are the six corners of the feasible region, and vectors $\boldsymbol{v}_{\alpha\beta0} = \boldsymbol{v}_{\alpha\beta7}$ are two zero vectors. The voltage $\boldsymbol{v}_{\alpha\beta}$ is expressed as a linear combination of two adjacent achievable vectors and the two zero vectors. For example, vector $\boldsymbol{v}_{\alpha\beta}$ in fig. 3.3 would be decomposed into

$$\boldsymbol{v}_{\alpha\beta} = t_0'\boldsymbol{v}_{\alpha\beta0} + t_1'\boldsymbol{v}_{\alpha\beta1} + t_2'\boldsymbol{v}_{\alpha\beta2}, \tag{3.1}$$

$$1 = t_0' + t_1' + t_3'. \tag{3.2}$$

The coefficients are then scaled by the SVM sampling period T_{svm} to $t_0 = t_0'T_{\text{svm}}$, $t_1 = t_1'T_{\text{svm}}$, $t_2 = t_2'T_{\text{svm}}$. The scaled coefficients define the time duration the achievable voltage vectors are applied to the motor during the sampling period. Both zero vectors $\boldsymbol{v}_{\alpha\beta0}$ and $\boldsymbol{v}_{\alpha\beta7}$ can be used and the order at which the achievable vectors are applied is chosen such that the number of switching events is minimized [12].

The SVM yields lower harmonic distortion than PWM with zero common-mode voltage [19]. However, as mentioned in [11] and shown in [19], the common-mode voltage can be chosen such that symmetrical PWM outputs the same switching signals as SVM. This common-mode is obtained as

$$v_{\text{cms}} = -\frac{1}{2}\left(\min(\boldsymbol{v}_{\text{abc}}) + \max(\boldsymbol{v}_{\text{abc}})\right), \tag{3.3}$$

which also ensures full utilization of the inverter voltage range. The continuous-control-set algorithms examined in this thesis were combined with symmetrical PWM and common-mode injection defined by (3.3).

k	$v_{\mathrm{a}k}$	$v_{\mathrm{b}k}$	$v_{\mathrm{c}k}$	$v_{\alpha k}$	$v_{\beta k}$
0	$-\frac{1}{2}v_{\mathrm{dc}}$	$-\frac{1}{2}v_{\mathrm{dc}}$	$-\frac{1}{2}v_{\mathrm{dc}}$	0	0
1	$+\frac{1}{2}v_{\mathrm{dc}}$	$-\frac{1}{2}v_{\mathrm{dc}}$	$-\frac{1}{2}v_{\mathrm{dc}}$	$+\frac{2}{3}v_{\mathrm{dc}}$	0
2	$+\frac{1}{2}v_{\mathrm{dc}}$	$+\frac{1}{2}v_{\mathrm{dc}}$	$-\frac{1}{2}v_{\mathrm{dc}}$	$+\frac{1}{3}v_{\mathrm{dc}}$	$+\frac{1}{\sqrt{3}}v_{\mathrm{dc}}$
3	$-\frac{1}{2}v_{\mathrm{dc}}$	$+\frac{1}{2}v_{\mathrm{dc}}$	$-\frac{1}{2}v_{\mathrm{dc}}$	$-\frac{1}{3}v_{\mathrm{dc}}$	$+\frac{1}{\sqrt{3}}v_{\mathrm{dc}}$
4	$-\frac{1}{2}v_{\mathrm{dc}}$	$+\frac{1}{2}v_{\mathrm{dc}}$	$+\frac{1}{2}v_{\mathrm{dc}}$	$-\frac{2}{3}v_{\mathrm{dc}}$	0
5	$-\frac{1}{2}v_{\mathrm{dc}}$	$-\frac{1}{2}v_{\mathrm{dc}}$	$+\frac{1}{2}v_{\mathrm{dc}}$	$-\frac{1}{3}v_{\mathrm{dc}}$	$-\frac{1}{\sqrt{3}}v_{\mathrm{dc}}$
6	$+\frac{1}{2}v_{\mathrm{dc}}$	$-\frac{1}{2}v_{\mathrm{dc}}$	$+\frac{1}{2}v_{\mathrm{dc}}$	$+\frac{1}{3}v_{\mathrm{dc}}$	$-\frac{1}{\sqrt{3}}v_{\mathrm{dc}}$
7	$+\frac{1}{2}v_{\mathrm{dc}}$	$+\frac{1}{2}v_{\mathrm{dc}}$	$+\frac{1}{2}v_{\mathrm{dc}}$	0	0

Table 3.1: The achievable vectors $\boldsymbol{v}_{\alpha\beta k}$ and corresponding $\boldsymbol{v}_{\mathrm{abc}k}$ vectors.

3.3 PI Controller

As the PI controller is single-input, single-output (SISO), the cascaded multi-loop control structure is employed. A general discrete-time PI controller without anti-windup assigns control $u(k)$ to error signal

$$e(k) = y_{\mathrm{ref}}(k) - y(k) \tag{3.4}$$

as follows

$$\begin{aligned} u(k) &= u_{\mathrm{p}}(k) + u_{\mathrm{i}}(k), && (3.5)\\ u_{\mathrm{p}}(k) &= K_{\mathrm{p}} e(k), && (3.6)\\ u_{\mathrm{i}}(k) &= u_{\mathrm{i}}(k-1) + \frac{K_{\mathrm{i}}}{T_{\mathrm{s}}} e(k). && (3.7) \end{aligned}$$

The constant K_{i} is scaled by the controller sampling period T_{s}. The control law changes to the following form when output saturation and simple clamping anti-windup is implemented

$$\begin{aligned} u(k) &= \max\left\{\min\left\{u_{\mathrm{p}}(k) + u_{\mathrm{i}}(k-1),\, u_{\max}\right\},\, u_{\min}\right\} && (3.8)\\ u_{\mathrm{p}}(k) &= K_{\mathrm{p}} e(k), && (3.9)\\ u_{\mathrm{i}}(k) &= \begin{cases} u_{\mathrm{i}}(k-1) + \dfrac{K_{\mathrm{i}}}{T_{\mathrm{s}}} e(k) & \text{for } u(k) = u_{\mathrm{p}}(k) + u_{\mathrm{i}}(k-1), \\ u_{\mathrm{i}}(k-1) & \text{otherwise.} \end{cases} && (3.10) \end{aligned}$$

In this formulation, the effect of integral action is delayed by one sample to avoid algebraic loop.

The DQ currents are controlled independently and the controller G_1 consists of two separate PI controllers. The velocity controller G_2 outputs the reference value for the quadrature

current for controller G_1, and the direct current is commanded to zero. The position controller G_3 outputs the reference velocity. The constraints were relaxed to $|i_\mathrm{d}| < I_\mathrm{max}$ and $|i_\mathrm{q}| < I_\mathrm{max}$, $|v_\mathrm{d}| < V_\mathrm{max}$ and $|v_\mathrm{q}| < V_\mathrm{max}$ and implemented using saturation blocks.

3.4 Continuous-Control-Set Model Predictive Control

3.4.1 Single-Loop

CCS-MPC formulates the control task as an optimization problem. The following formulation of convex quadratic program with linear constraints was chosen

$$\min_{\boldsymbol{z}} \sum_{k=0}^{N-1} (\boldsymbol{y}_{k+1} - \boldsymbol{r}_{k+1})^\mathrm{T} \boldsymbol{Q} (\boldsymbol{y}_{k+1} - \boldsymbol{r}_{k+1}) + \Delta \boldsymbol{u}_k^\mathrm{T} \boldsymbol{R} \Delta \boldsymbol{u}_k \tag{3.11a}$$

$$\text{s.t.} \quad \boldsymbol{x}_{k+1} = \boldsymbol{A}\boldsymbol{x}_k + \boldsymbol{B}\boldsymbol{u}_k, \tag{3.11b}$$

$$\boldsymbol{y}_{k+1} = \boldsymbol{C}\boldsymbol{x}_{k+1}, \tag{3.11c}$$

$$\boldsymbol{P}_x \boldsymbol{x}_{k+1} \leq \boldsymbol{p}_x, \tag{3.11d}$$

$$\boldsymbol{P}_u \boldsymbol{u}_k \leq \boldsymbol{p}_u, \tag{3.11e}$$

$$\boldsymbol{z} = \begin{bmatrix} \boldsymbol{u}_0^\mathrm{T} & \boldsymbol{u}_1^\mathrm{T} & \dots & \boldsymbol{u}_{N-1}^\mathrm{T} \end{bmatrix}^\mathrm{T}, \tag{3.11f}$$

$$\Delta \boldsymbol{u}_k = \boldsymbol{u}_k - \boldsymbol{u}_{k-1}, \tag{3.11g}$$

$$\boldsymbol{x}_0 = \boldsymbol{x}(t), \tag{3.11h}$$

$$\boldsymbol{u}_{-1} = \boldsymbol{u}(t - T_\mathrm{s}), \tag{3.11i}$$

$$\boldsymbol{r}_{k+1} = \boldsymbol{r}(t + kT_\mathrm{s}), \tag{3.11j}$$

where weighting matrix $\boldsymbol{Q}$ is symmetric and positive semidefinite and weighting matrix $\boldsymbol{R}$ is symmetric and positive definite. $\boldsymbol{P}_x$, $\boldsymbol{p}_x$, $\boldsymbol{P}_u$, $\boldsymbol{p}_u$ are given by (2.140) and (2.155), and N is the prediction horizon. In this formulation, the control horizon is the same as prediction horizon. The controller operates with sampling period T_s and the control law is as follows. At time t, state $x(t)$ is measured and system matrix $\boldsymbol{A}$ is obtained by discretizing (2.107), which is parametrized by ω. Matrices $\boldsymbol{B}$ and $\boldsymbol{C}$ stay fixed. The controller then finds optimal sequence $\boldsymbol{z}$, from which only $\Delta \boldsymbol{u}_0$ is taken to compute $\boldsymbol{u}_0 = \boldsymbol{u}_{-1} + \Delta \boldsymbol{u}_0$. The voltage vector $\boldsymbol{u}_0$ is then applied to the motor and saved for the next sampling period. If the reference output $\boldsymbol{r}$ is given for the next sampling period $\boldsymbol{r}(t + T_\mathrm{s})$ only, constant reference over the whole prediction horizon is assumed, i.e. $\boldsymbol{r}_{k+1} = \boldsymbol{r}(t + T_\mathrm{s})$.

The above formulation of the optimization problem can be expressed in condensed form,

in which the predicted state is eliminated. The condensed form is

$$\min_{\boldsymbol{z}} \quad \frac{1}{2}\boldsymbol{z}^{\mathrm{T}}\boldsymbol{H}\boldsymbol{z} + \begin{bmatrix}\boldsymbol{x}_0^{\mathrm{T}} & \boldsymbol{u}_{-1}^{\mathrm{T}} & \boldsymbol{r}_1^{\mathrm{T}} & \boldsymbol{r}_2^{\mathrm{T}} & \dots & \boldsymbol{r}_N^{\mathrm{T}}\end{bmatrix}\boldsymbol{F}^{\mathrm{T}}\boldsymbol{z} \tag{3.12a}$$

$$\text{s.t.} \quad \boldsymbol{G}\boldsymbol{z} \leq \boldsymbol{W} + \boldsymbol{S}\boldsymbol{x}_0, \tag{3.12b}$$

$$\boldsymbol{z} = \begin{bmatrix}\boldsymbol{u}_0^{\mathrm{T}} & \boldsymbol{u}_1^{\mathrm{T}} & \dots & \boldsymbol{u}_{N-1^{\mathrm{T}}}\end{bmatrix}^{\mathrm{T}}, \tag{3.12c}$$

$$\boldsymbol{x}_0 = \boldsymbol{x}(t), \tag{3.12d}$$

$$\boldsymbol{u}_{-1} = \boldsymbol{u}(t - T_{\mathrm{s}}), \tag{3.12e}$$

$$\boldsymbol{r}_k = \boldsymbol{r}(t + kT_{\mathrm{s}}), \quad k = 1, 2, \dots, N, \tag{3.12f}$$

where matrices $\boldsymbol{H}$, $\boldsymbol{F}$, $\boldsymbol{G}$, $\boldsymbol{W}$, $\boldsymbol{S}$ are derived in appendix B. To obtain solution, this formulation can be easily plugged into standard QP solvers. Choice of matrix $\boldsymbol{C}$ determines reference outputs to be tracked.

3.4.2 Cascaded

In cascaded structure, controller G_1 is chosen to be the above stated CCS-MPC with

$$\boldsymbol{C} = \begin{bmatrix}1 & 0 & 0 & 0\\ 0 & 1 & 0 & 0\end{bmatrix}. \tag{3.13}$$

Thus, G_1 controls the DQ currents. Controllers G_2 and G_3 are merged together into CCS-MPC applied to the mechanical equations

$$\dot{\boldsymbol{x}} = \boldsymbol{A}_{\mathrm{c}}\boldsymbol{x} + \boldsymbol{B}_{\mathrm{c}}\boldsymbol{u}, \tag{3.14}$$

$$\boldsymbol{A}_{\mathrm{c}} = \begin{bmatrix}-\dfrac{B}{J} & 0\\ 1 & 0\end{bmatrix}, \quad \boldsymbol{B}_{\mathrm{c}} = \begin{bmatrix}\dfrac{3K_{\mathrm{b}}}{2J}\\ 0\end{bmatrix}, \tag{3.15}$$

$$\boldsymbol{x} = \begin{bmatrix}\omega & \theta\end{bmatrix}^{\mathrm{T}} \tag{3.16}$$

$$\boldsymbol{u} = \begin{bmatrix}i_{\mathrm{q}}\end{bmatrix}. \tag{3.17}$$

Based on choice of the output matrix, one can control position or velocity (or both).

3.5 Finite-Control-Set Model Predictive Control

FCS-MPC formulates the control task almost identically as CCS-MPC:

$$\min_{\boldsymbol{z}} \sum_{k=0}^{N-1} (\boldsymbol{y}_{k+1} - \boldsymbol{r}_{k+1})^{\mathrm{T}} \boldsymbol{Q} (\boldsymbol{y}_{k+1} - \boldsymbol{r}_{k+1}) + \Delta \boldsymbol{u}_k^{\mathrm{T}} \boldsymbol{R} \Delta \boldsymbol{u}_k \tag{3.18a}$$

$$\text{s.t.} \quad \boldsymbol{x}_{k+1} = \boldsymbol{A}\boldsymbol{x}_k + \boldsymbol{B}\boldsymbol{u}_k, \tag{3.18b}$$

$$\boldsymbol{y}_{k+1} = \boldsymbol{C}\boldsymbol{x}_{k+1}, \tag{3.18c}$$

$$\boldsymbol{P}_x \boldsymbol{x}_{k+1} \leq \boldsymbol{p}_x, \tag{3.18d}$$

$$\boldsymbol{u}_k \in \mathbb{U} \tag{3.18e}$$

$$\boldsymbol{z} = \begin{bmatrix} \boldsymbol{u}_0{}^{\mathrm{T}} & \boldsymbol{u}_1{}^{\mathrm{T}} & \dots & \boldsymbol{u}_{N-1}^{\mathrm{T}} \end{bmatrix}^{\mathrm{T}}, \tag{3.18f}$$

$$\Delta \boldsymbol{u}_k = \boldsymbol{u}_k - \boldsymbol{u}_{k-1}, \tag{3.18g}$$

$$\boldsymbol{x}_0 = \boldsymbol{x}(t), \tag{3.18h}$$

$$\boldsymbol{u}_{-1} = \boldsymbol{u}(t - T_{\mathrm{s}}), \tag{3.18i}$$

$$\boldsymbol{r}_{k+1} = \boldsymbol{r}(t + kT_{\mathrm{s}}). \tag{3.18j}$$

The main difference is that $\boldsymbol{u}_k$ belongs to a finite set of vectors

$$\mathbb{U} = \left\{ \begin{bmatrix} +\frac{1}{2} \\ +\frac{1}{2} \\ +\frac{1}{2} \end{bmatrix}, \begin{bmatrix} +\frac{1}{2} \\ +\frac{1}{2} \\ -\frac{1}{2} \end{bmatrix}, \begin{bmatrix} +\frac{1}{2} \\ -\frac{1}{2} \\ +\frac{1}{2} \end{bmatrix}, \begin{bmatrix} +\frac{1}{2} \\ -\frac{1}{2} \\ -\frac{1}{2} \end{bmatrix}, \begin{bmatrix} -\frac{1}{2} \\ +\frac{1}{2} \\ +\frac{1}{2} \end{bmatrix}, \begin{bmatrix} -\frac{1}{2} \\ +\frac{1}{2} \\ -\frac{1}{2} \end{bmatrix}, \begin{bmatrix} -\frac{1}{2} \\ -\frac{1}{2} \\ +\frac{1}{2} \end{bmatrix}, \begin{bmatrix} -\frac{1}{2} \\ -\frac{1}{2} \\ -\frac{1}{2} \end{bmatrix} \right\}, \tag{3.19}$$

where each vector describes one switching combination in the inverter. Each element of the vectors corresponds to one phase-leg in the inverter, where $+1/2$ means it is connected to $+v_{\mathrm{dc}}/2$ and -1/2 means it is connected to $-v_{\mathrm{dc}}/2$. Matrix $\boldsymbol{B}$ is therefore obtained by discretizing $\boldsymbol{B}_{\mathrm{c}}\tilde{\boldsymbol{R}}\tilde{\boldsymbol{K}}v_{\mathrm{dc}}$, which is the continuous-time input matrix multiplied by the reduced Park and Clarke transformation matrices and by DC-bus voltage. In this formulation, the 2-norm squared $\|\Delta \boldsymbol{u}_k\|_2^2$ is equal to the number of switching transitions that happen during step from time $k-1$ to k. As there is usually no reason to penalize some switches of the inverter more than others, one usually chooses $\boldsymbol{R} = \lambda \boldsymbol{I}$, where λ is a scalar weighting parameter. This parameter penalizes the switching events and, thus, it can be used to tune the average steady-state switching frequency. This is problem can be solved by enumerating all possible sequence of the input vector. However, number of such sequences is 8^N, which makes the exhaustive search a feasible option only for very short prediction horizons.

FCS-MPC can also be expressed in a condensed form as

$$\min_{\boldsymbol{z}} \quad \frac{1}{2}\boldsymbol{z}^{\mathrm{T}}\boldsymbol{H}\boldsymbol{z} + \begin{bmatrix}\boldsymbol{x}_0^{\mathrm{T}} & \boldsymbol{u}_{-1}^{\mathrm{T}} & \boldsymbol{r}_1^{\mathrm{T}} & \boldsymbol{r}_2^{\mathrm{T}} & \dots & \boldsymbol{r}_N^{\mathrm{T}}\end{bmatrix}\boldsymbol{F}^{\mathrm{T}}\boldsymbol{z} \tag{3.20a}$$

$$\text{s.t.} \quad \boldsymbol{G}\boldsymbol{z} \leq \boldsymbol{W} + \boldsymbol{S}\boldsymbol{x}_0, \tag{3.20b}$$

$$\boldsymbol{z} = \begin{bmatrix}\boldsymbol{u}_0^{\mathrm{T}} & \boldsymbol{u}_1^{\mathrm{T}} & \dots & \boldsymbol{u}_{N-1^{\mathrm{T}}}\end{bmatrix}^{\mathrm{T}}, \tag{3.20c}$$

$$\boldsymbol{u}_k \in \mathbb{U}, \tag{3.20d}$$

$$\boldsymbol{x}_0 = \boldsymbol{x}(t), \tag{3.20e}$$

$$\boldsymbol{u}_{-1} = \boldsymbol{u}(t - T_{\mathrm{s}}), \tag{3.20f}$$

$$\boldsymbol{r}_k = \boldsymbol{r}(t + kT_{\mathrm{s}}), \quad k = 1, 2, \dots, N, \tag{3.20g}$$

where the definition of some matrices slightly differs from CCS-MPC. In [11], reformulation of the problem using the unconstrained solution and Cholesky decomposition of the hessian matrix $\boldsymbol{H}$ is given. This changes the branching factor from 8 to 2, while increasing the depth of the tree three times. Also it enables application of branch and bound method called sphere decoding which allows effective search in the tree if close-to-optimal solution is available. More details are in [11]. Here, the initial guess of the close-to-optimal solution was modified in order to account for constraints imposed on the DQ currents. The initial guess was obtained by sequential solution of one-step FCS-MPC.

Chapter 4

Simulation

This chapter evaluates the control algorithms in simulation. The continuous-control-set algorithms were combined with symmetrical PWM with SVM equivalent common-mode voltage injection. Other nonidealities, such as measurement noise and model uncertainty, were not considered. The reference is assumed to be known in advance and the controllers may anticipate it.

4.1 Chosen Parameters

The sampling frequencies and prediction horizons were chosen such that the controllers fit the capabilities of the platform chosen for hardware evaluation. Other tuning parameters of the control algorithms were chosen such that the controllers give similar steady-state torque ripple. The exact values are not of great importance because the goal of this chapter is not to find the best controller, but rather to describe the main characteristics.

4.1.1 PI Controller

The current loop of the PI controller was designed to operate at $T_{\mathrm{s1}} = 25\,\mathrm{kHz}$ the the proportional constant was tuned to 20.3 and the integral constant was tuned to $0.95T_{\mathrm{s1}}$ (the units of the constants are omitted). The velocity controller was designed to operate at $T_{\mathrm{s2}} = 1\,\mathrm{kHz}$ with the proportional constant 1.2 and the integral constant $0.04T_{\mathrm{s2}}$. The position controller operates at 100 Hz the proportional constant 50 and the integral constant 0 (the integral action is not necessary because the position is the integral of velocity).

4.1.2 CCS-MPC

Single-loop CCS-MPC was chosen to operate at 25 kHz and two lengths 5 and 10 of the prediction horizon were tested. In the cascaded structure, the inner loop operated at 25 kHz and the outer one at 1 kHz.

4.1.3 FCS-MPC

The evaluation was done with the sampling frequency of 500 kHz and prediction horizon 3.

4.2 Current Control

Tracking of reference current was tested at velocity of $307\,\mathrm{rad\,s^{-1}}$ (2900 RPM) by commanding the direct current to zero and the quadrature current from steady-state value of 2 A to 3 A. The steady state current compensated for nonzero load torque of $-0.065\,\mathrm{N\,m}$. Also, to find the effects of the external torque on the current controllers, a step change of the load torque from -0.065 to -0.2 was introduced. The results in fig. 4.1 show that all three algorithms control the DQ currents as required — the qudrature current tracks the reference and the direct current stays close to zero.

Even though PI controller is very simple to implement, it provides very good results when properly tuned. The main drawback is that the constrained are not properly imposed. The choice of the relaxed constraints is justified here by the control of the direct current close to zero.

The anticipation of the reference is apparent in the response of CCS-MPC. The small overshoot could be eliminated by choosing longer prediction horizon. However, with short prediction horizon, it is difficult to completely remove the overshoot.

FCS-MPC also anticipates the reference but on much smaller time interval because it operates at much higher sampling rate. It has also the fastest response to the step-change in reference. The current ripple is not uniform, which results in wider spectrum of frequencies in the phase currents. This can be fixed by choosing longer prediction horizon. Doing so results in more uniform torque ripple. Another interesting result is that the number of nodes FCS-MPC visit during the search for optimal control is greater during transients and small during steady state, see fig. 4.2.

The step change in the load torque happened at time 1×10^{-3} and it had no direct effect on the DQ currents. However, it indirectly influences them by increasing or decreasing the angular velocity.

4.3 Velocity Control

Reference velocity tracking was tested by setting the reference velocity to $10\,\mathrm{rad\,s^{-1}}$ (95 RPM) from zero state. A step-change of the external load torque from 0 to $-0.05\,\mathrm{N\,m}$ was applied. It turned out to be perhaps impossible to tune the FCS-MPC for velocity tracking and all attempts gave unstable closed-loop. The reason is probably high sampling frequency relative to the velocity response. Thus, FCS-MPC is excluded from the analysis. As shown in fig. 4.3, all controllers tracked the velocity reference up to the step in the external load. The constant torque disturbance was rejected only by the PI controller because it is the only controller with integral action. Although the MPC cost function penalizes $\Delta \boldsymbol{u}$, it does not have integral action and thus the steady-state error when the external torque was applied. There are variants of MPC that reject constant disturbance, but they are not considered here. Note that the reference on the quadrature current is available only for the cascaded structures.

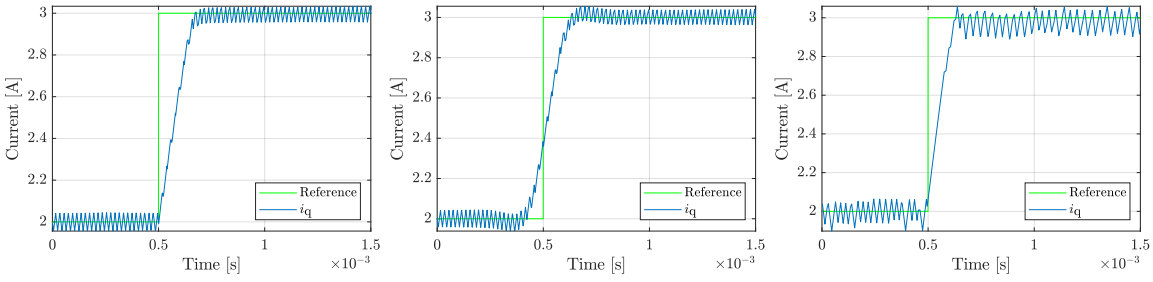

(a) PI control of i_q. **(b)** CCS-MPC control of i_q. **(c)** FCS-MPC control of i_q.

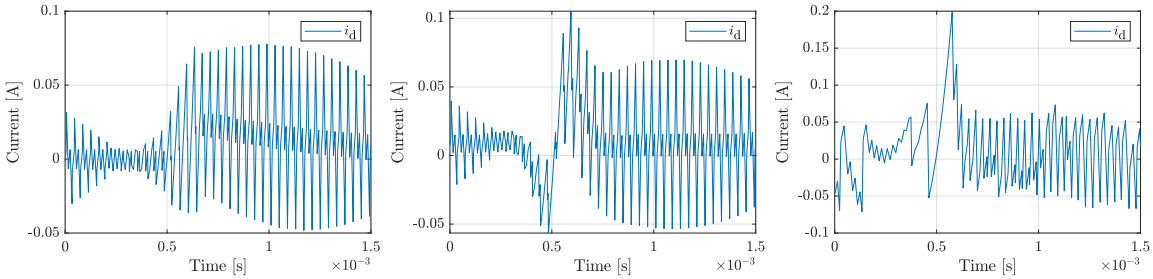

(d) PI control of i_d. **(e)** CCS-MPC control of i_d. **(f)** FCS-MPC control of i_d.

Figure 4.1: Control of the DQ currents.

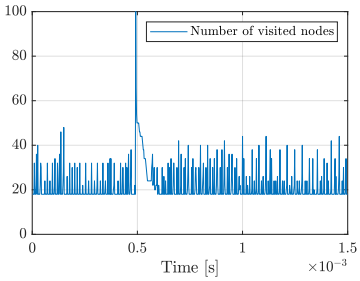

Figure 4.2: The number of nodes visited by FCS-MPC.

The single-loop CCS-MPC showed the fastest response.

4.4 Position Control

Position control using single-loop fast CCS-MPC turned out to be challenging and is therefore excluded. The PI and cascaded FCS-MPC responses are in fig. 4.4. The overshoot of the FCS-MPC could be reduced if properly tuned.

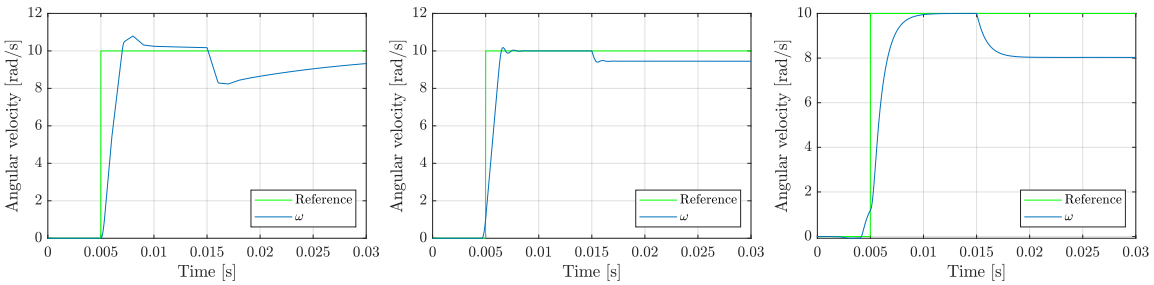

(a) PI controller, ω. **(b)** CCS-MPC, ω. **(c)** Cascaded CCS-MPC, ω.

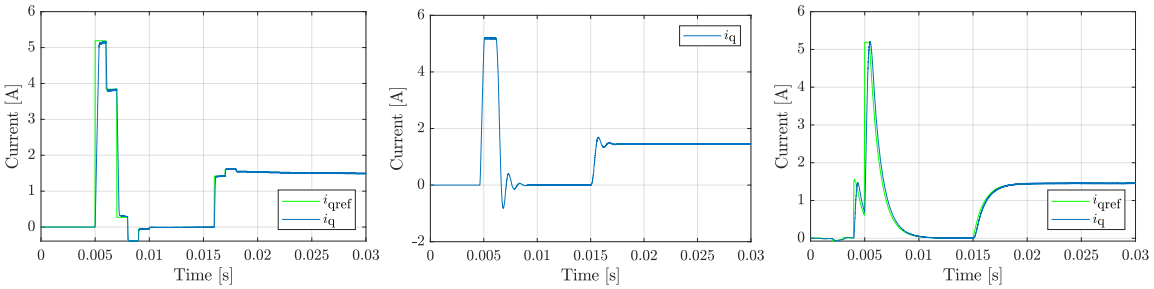

(d) PI controller, i_q. **(e)** CCS-MPC, i_q. **(f)** Cascaded CCS-MPC, i_q.

Figure 4.3: Velocities and quadrature currents durint velocity tracking.

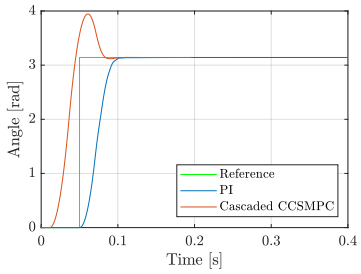

Figure 4.4: Position tracking.

Chapter 5

Hardware Implementation

To verify the algorithms discussed in the previous chapters on an actual PMSM, suitable commercially available platform was chosen. However, due to struggles with the hardware implementation, only field-oriented PI controller and one-step FCS-MPC were put into operation. Thus, the experimental evaluation is not provided and only general notes are given in this chapter.

5.1 Selected Hardware Platform

For hardware implementation, AD-FMCMOTCON2-EBZ driver by Analog devices together with ZedBoard was chosen. AD-FMCMOTCON2-EBZ is a driver system allowing control of two motors simultaneously. It contains sigma-delta modulators for measuring the phase currents with 16-bit resolution at 78.1 kHz. To measure at higher frequency, the resolution has to be decreased by decreasing decimation ration of demodulating filters. ZedBoard is a prototyping platform with Zynq-7000 system on a chip (SoC), which contains ARM® dual Cortex®-A9 and Xilinx 7-series field-programmable gate array (FPGA) fabric on a single chip. Both the ARM® processing system and FPGA fabric are supported by MATLAB and Simulink, and one can relatively easily implement co-designs both parts of the chip. A photograph of the platform is shown in fig. 5.1.

5.2 Bootstrap Circuit Limitations

One drawback of AD-FMCMOTCON2-EBZ driver is that uses bootstrap circuits to power the high-side switches. The board uses n-channel MOSFETs, which are switched when positive voltage is applied between the gate and source. When high-side MOSFET is switched, its source is connected to the DC-bus voltage and it is necessary to have voltage above this level to keep the switch on. One possibility is to use a bootstrap capacitor which is charged when the high-side MOSFET is off and the low-side MOSFET on, and provides sufficient voltage level when it is the other way around. However, the bootstrap capacitor gets discharged after some time (typically a few milliseconds) when the high-side MOSFET is kept on. This limits the maximum admissible duty cycle when a modulation stage is used. In principle, FCS-MPC may keep the high-side switches on indefinitely and the bootstrap capacitor should be taken into account. A very simple but not efficient solution is to override the controller switching sequence when a high-side MOSFET is on for too long [20].

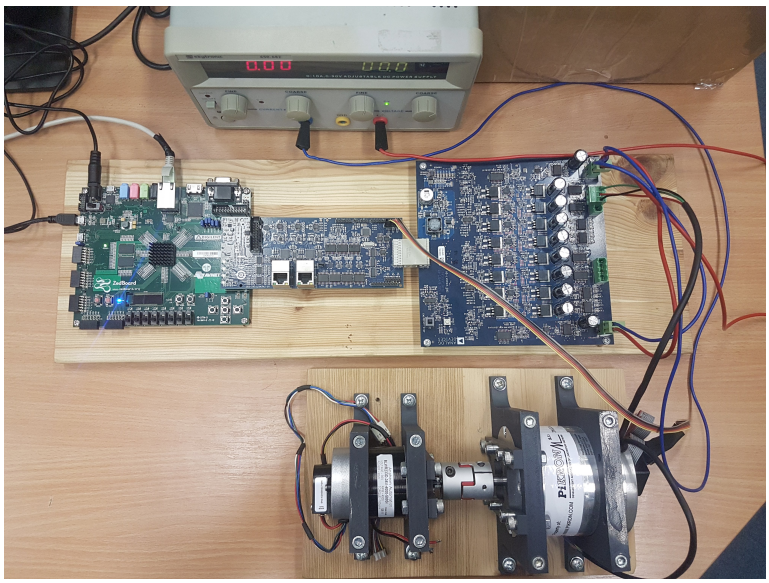

Figure 5.1: ZedBoard and AD-FMCMOTCON2-EBZ with two coupled PMSMs.

To avoid problems with the bootstrap capacitor, an attempt was to modify AD-FMCMOTCON2-EBZ driver by adding charge pumps, which would allow the high-side switches to be on indefinitely. However, the output voltages of the charge pumps dropped significantly when loaded and this solution did not work.

5.3 Delay Compensation

As the MPC algorithms are computationally demanding and it takes some time to obtain the result of the optimization problem, delay compensation should be implemented. A simple method is presented in **computationally demanding**. The idea is to delay the control input and apply it at the beginning of the next sampling period. The controller then uses state predicted for the next step instead of the current state.

Chapter 6

Conclusion

This thesis describes the mathematical model of PMSM and analyzes three control algorithms for this type of motor. All three of them, the field-oriented PI controller, CCS-MPC, and FCS-MPC, were capable of current control. For the velocity control, however, it turned out that it is difficult to design a stable closed-loop with FCS-MPC. This is a general problem in systems with both fast and slow dynamics. In PMSM, the electrical part requires fast controller as the electrical time constant is small. The mechanical one is usually greater and cascaded control structures are more suitable. However, when voltage modulation stage is used, it is possible to design single-loop velocity controller. To design stable position controller for used PMSM, it turned out that the cascaded structure is required.

Appendix A

Notes on PMSM Model

A.1 Derivation of Electromagnetic Torque

The electromagnetic torque generated by the phase currents is now derived using the law of conservation of energy

$$W_{\mathrm{el}} + W_{\mathrm{ex}} \;=\; W_{\mathrm{res}} + W_{\mathrm{fr}} + W_{\mathrm{field}} + W_{\mathrm{kin}}, \tag{A.1}$$

where W_{el} is the overall energy supplied by the electrical power supplies, W_{ex} is the overall energy supplied by external mechanical sources, W_{res} is the energy dissipated on the winding resistances, W_{fr} is the energy dissipated due to mechanical friction, W_{field} is the energy stored in the magnetic field, and W_{kin} is the kinetic energy stored in the rotor motion. Since eq. (A.1) holds at each time instant, it can be differentiated and expressed in terms of power

$$P_{\mathrm{el}} + P_{\mathrm{ex}} \;=\; P_{\mathrm{res}} + P_{\mathrm{fr}} + P_{\mathrm{field}} + P_{\mathrm{kin}}, \tag{A.2}$$

where each power term is the time derivative of corresponding energy. The external power P_{ex} taken with negative sign is the output power of the motor, i.e. the mechanical power supplied by the motor. Multiplying (2.2) by $\boldsymbol{i}_{\mathrm{abc}}^{\mathrm{T}}$ from the left and (2.41) by ω gives two power equations

$$\boldsymbol{i}_{\mathrm{abc}}^{\mathrm{T}}\boldsymbol{v}_{\mathrm{abc}} \;=\; R_{\mathrm{s}}\boldsymbol{i}_{\mathrm{abc}}^{\mathrm{T}}\boldsymbol{i}_{\mathrm{abc}} + \boldsymbol{i}_{\mathrm{abc}}^{\mathrm{T}}\frac{\mathrm{d}}{\mathrm{d}t}\boldsymbol{\psi}_{\mathrm{abc}}, \tag{A.3}$$

$$J\omega\frac{\mathrm{d}\omega}{\mathrm{d}t} \;=\; \omega\tau_{\mathrm{el}} + \omega\tau_{\mathrm{fr}} + \omega\tau_{\mathrm{cog}} + \omega\tau_{\mathrm{ex}}. \tag{A.4}$$

Defining

$$P_{\mathrm{el}} \;=\; \frac{\mathrm{d}W_{\mathrm{el}}}{\mathrm{d}t} \;=\; \boldsymbol{i}_{\mathrm{abc}}^{\mathrm{T}}\boldsymbol{v}_{\mathrm{abc}}, \tag{A.5}$$

$$P_{\mathrm{ex}} \;=\; \frac{\mathrm{d}W_{\mathrm{ex}}}{\mathrm{d}t} \;=\; \omega\tau_{\mathrm{cog}} + \omega\tau_{\mathrm{ex}}, \tag{A.6}$$

$$P_{\mathrm{res}} \;=\; \frac{\mathrm{d}W_{\mathrm{res}}}{\mathrm{d}t} \;=\; R_{\mathrm{s}}\boldsymbol{i}_{\mathrm{abc}}^{\mathrm{T}}\boldsymbol{i}_{\mathrm{abc}}, \tag{A.7}$$

$$P_{\mathrm{fr}} \;=\; \frac{\mathrm{d}W_{\mathrm{fr}}}{\mathrm{d}t} \;=\; -\omega\tau_{\mathrm{fr}}, \tag{A.8}$$

$$P_{\mathrm{kin}} \;=\; \frac{\mathrm{d}W_{\mathrm{kin}}}{\mathrm{d}t} \;=\; J\omega\frac{\mathrm{d}\omega}{\mathrm{d}t}, \tag{A.9}$$

substracting (A.4) from (A.3) and rearranging yields

$$P_{\mathrm{el}} + P_{\mathrm{ex}} \;=\; P_{\mathrm{res}} + P_{\mathrm{fr}} + P_{\mathrm{kin}} + \boldsymbol{i}_{\mathrm{abc}}^{\mathrm{T}} \frac{\mathrm{d}}{\mathrm{d}t} \boldsymbol{\psi}_{\mathrm{abc}} - \omega \tau_{\mathrm{el}}. \tag{A.10}$$

By comparing (A.10) and (A.2), it can be stated that

$$P_{\mathrm{field}} \;=\; \frac{\mathrm{d}W_{\mathrm{field}}}{\mathrm{d}t} \;=\; \boldsymbol{i}_{\mathrm{abc}}^{\mathrm{T}} \frac{\mathrm{d}}{\mathrm{d}t} \boldsymbol{\psi}_{\mathrm{abc}} - \omega \tau_{\mathrm{el}}, \tag{A.11}$$

which is further modified using (2.4), (2.5), and (2.9) as

$$\frac{\mathrm{d}W_{\mathrm{field}}}{\mathrm{d}t} \;=\; \boldsymbol{i}_{\mathrm{abc}}^{\mathrm{T}} \frac{\mathrm{d}}{\mathrm{d}t} \left(\boldsymbol{L} \boldsymbol{i}_{\mathrm{abc}} \right) + \boldsymbol{i}_{\mathrm{abc}}^{\mathrm{T}} \boldsymbol{e}_{\mathrm{abc}} - \omega \tau_{\mathrm{el}} \tag{A.12}$$

The magnetic field in the motor is fully determined by the stator currents and the rotor angle alone. Thus, the energy stored in the magnetic field can be expressed as a function of the phase currents and the rotor angle $W_{\mathrm{field}}(i_{\mathrm{a}}, i_{\mathrm{b}}, i_{\mathrm{c}}, \theta)$ and it does not depend on the rotor velocity. For this reason, W_{field} can be derived by setting $\theta = \mathrm{const}$ and $\omega = 0$, which gives

$$\left. \frac{\mathrm{d}W_{\mathrm{field}}}{\mathrm{d}t} \right|_{\theta = \mathrm{const}} \;=\; \boldsymbol{i}_{\mathrm{abc}}^{\mathrm{T}} \left. \frac{\mathrm{d}\boldsymbol{L} \boldsymbol{i}_{\mathrm{abc}}}{\mathrm{d}t} \right|_{\theta = \mathrm{const}} \tag{A.13}$$

and upon integrating

$$W_{\mathrm{field}} \;=\; \frac{1}{2} \boldsymbol{i}_{\mathrm{abc}}^{\mathrm{T}} \boldsymbol{L} \boldsymbol{i}_{\mathrm{abc}}. \tag{A.14}$$

Note that the symmetry property of the inductance matrix $\boldsymbol{L}$ was used. Now the rate of change of W_{field} is expressed as

$$\frac{\mathrm{d}W_{\mathrm{field}}}{\mathrm{d}t} \;=\; \frac{\partial W_{\mathrm{field}}}{\partial \boldsymbol{i}_{\mathrm{abc}}} \frac{\mathrm{d}\boldsymbol{i}_{\mathrm{abc}}}{\mathrm{d}t} + \frac{\partial W_{\mathrm{field}}}{\partial \theta} \frac{\mathrm{d}\theta}{\mathrm{d}t}, \tag{A.15}$$

where

$$\frac{\partial W_{\mathrm{field}}}{\partial \boldsymbol{i}_{\mathrm{abc}}} \;=\; \begin{bmatrix} \frac{\partial W_{\mathrm{field}}}{\partial i_{\mathrm{a}}} & \frac{\partial W_{\mathrm{field}}}{\partial i_{\mathrm{b}}} & \frac{\partial W_{\mathrm{field}}}{\partial i_{\mathrm{c}}} \end{bmatrix}. \tag{A.16}$$

From (A.11) and using the fact that the stator flux linkages $\boldsymbol{\psi}_{\mathrm{abc}}$ are also functions of the stator currents and the rotor angle it follows that

$$\frac{\mathrm{d}W_{\mathrm{field}}}{\mathrm{d}t} \;=\; \boldsymbol{i}_{\mathrm{abc}}^{\mathrm{T}} \left(\frac{\partial \boldsymbol{\psi}_{\mathrm{abc}}}{\partial \boldsymbol{i}_{\mathrm{abc}}} \frac{\mathrm{d}\boldsymbol{i}_{\mathrm{abc}}}{\mathrm{d}t} + \frac{\partial \boldsymbol{\psi}_{\mathrm{abc}}}{\partial \theta} \frac{\mathrm{d}\theta}{\mathrm{d}t} \right) - \omega \tau_{\mathrm{el}} \tag{A.17}$$

$$\;=\; \boldsymbol{i}_{\mathrm{abc}}^{\mathrm{T}} \frac{\partial \boldsymbol{\psi}_{\mathrm{abc}}}{\partial \boldsymbol{i}_{\mathrm{abc}}} \frac{\mathrm{d}\boldsymbol{i}_{\mathrm{abc}}}{\mathrm{d}t} + \left(\boldsymbol{i}_{\mathrm{abc}}^{\mathrm{T}} \frac{\partial \boldsymbol{\psi}_{\mathrm{abc}}}{\partial \theta} - \tau_{\mathrm{el}} \right) \frac{\mathrm{d}\theta}{\mathrm{d}t}, \tag{A.18}$$

where

$$\frac{\partial \boldsymbol{\psi}_{\mathrm{abc}}}{\partial \boldsymbol{i}_{\mathrm{abc}}} = \begin{bmatrix} \frac{\partial \psi_{\mathrm{a}}}{\partial i_{\mathrm{a}}} & \frac{\partial \psi_{\mathrm{a}}}{\partial i_{\mathrm{b}}} & \frac{\partial \psi_{\mathrm{a}}}{\partial i_{\mathrm{c}}} \\ \frac{\partial \psi_{\mathrm{b}}}{\partial i_{\mathrm{a}}} & \frac{\partial \psi_{\mathrm{b}}}{\partial i_{\mathrm{b}}} & \frac{\partial \psi_{\mathrm{b}}}{\partial i_{\mathrm{c}}} \\ \frac{\partial \psi_{\mathrm{c}}}{\partial i_{\mathrm{a}}} & \frac{\partial \psi_{\mathrm{c}}}{\partial i_{\mathrm{b}}} & \frac{\partial \psi_{\mathrm{c}}}{\partial i_{\mathrm{c}}} \end{bmatrix}. \tag{A.19}$$

Comparing the coefficients at the derivatives in (A.15) and (A.18) gives

$$\frac{\partial W_{\mathrm{field}}}{\partial \theta} = \boldsymbol{i}_{\mathrm{abc}}^{\mathrm{T}} \frac{\partial \boldsymbol{\psi}_{\mathrm{abc}}}{\partial \theta} - \tau_{\mathrm{el}}, \tag{A.20}$$

which is rewritten as

$$\tau_{\mathrm{el}} = \boldsymbol{i}_{\mathrm{abc}}^{\mathrm{T}} \frac{\partial \boldsymbol{\psi}_{\mathrm{abc}}}{\partial \theta} - \frac{\partial W_{\mathrm{field}}}{\partial \theta} \tag{A.21}$$

$$= \frac{\partial W_{\mathrm{field}}^{*}}{\partial \theta}, \tag{A.22}$$

where

$$W_{\mathrm{field}}^{*} = \boldsymbol{i}_{\mathrm{abc}}^{\mathrm{T}} \boldsymbol{\psi}_{\mathrm{abc}} - W_{\mathrm{field}} \tag{A.23}$$

$$= \frac{1}{2} \boldsymbol{i}_{\mathrm{abc}}^{\mathrm{T}} \boldsymbol{L} \boldsymbol{i}_{\mathrm{abc}} + \boldsymbol{i}_{\mathrm{abc}}^{\mathrm{T}} \boldsymbol{\psi}_{\mathrm{abcr}} \tag{A.24}$$

is the field co-energy. The resulting expression for the electromagnetic torque is

$$\tau_{\mathrm{el}} = \frac{1}{2} \boldsymbol{i}_{\mathrm{abc}}^{\mathrm{T}} \frac{\partial \boldsymbol{L}}{\partial \theta} \boldsymbol{i}_{\mathrm{abc}} + \frac{1}{\omega} \boldsymbol{i}_{\mathrm{abc}}^{\mathrm{T}} \boldsymbol{e}_{\mathrm{abc}}. \tag{A.25}$$

A.2 Notes on Clarke Transformation

The Clarke transformation matrix given in (2.55) can be written as

$$\boldsymbol{K} = \frac{2}{3} \begin{bmatrix} 1 & \cos\left(\frac{2\pi}{3}\right) & \cos\left(-\frac{2\pi}{3}\right) \\ 0 & \sin\left(\frac{2\pi}{3}\right) & \sin\left(-\frac{2\pi}{3}\right) \\ \frac{1}{2} & \frac{1}{2} & \frac{1}{2} \end{bmatrix}. \tag{A.26}$$

For balanced vectors, e.g. current vector $\boldsymbol{i}_{\mathrm{abc}}$, the γ component is zero and the α and β components are

$$\begin{bmatrix} i_{\alpha} \\ i_{\beta} \end{bmatrix} = i_{\mathrm{a}} \frac{2}{3} \begin{bmatrix} 1 \\ 0 \end{bmatrix} + i_{\mathrm{b}} \frac{2}{3} \begin{bmatrix} \cos\left(\frac{2\pi}{3}\right) \\ \sin\left(\frac{2\pi}{3}\right) \end{bmatrix} + i_{\mathrm{c}} \frac{2}{3} \begin{bmatrix} \cos\left(-\frac{2\pi}{3}\right) \\ \sin\left(-\frac{2\pi}{3}\right) \end{bmatrix}. \tag{A.27}$$

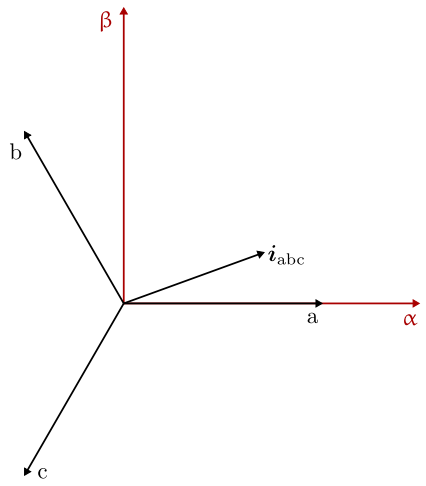

Figure A.1: Interpretation of Clarke transformation.

Thus, the Clarke transformation interprets balanced phase vectors as a linear combination of three basis vectors in a plane rotated by 120 degrees from each other and with magnitude of 2/3. The transformed components α and β are coordinates in an orthogonal reference frame as depicted in fig. A.1.

For balanced variables, Clarke transformation can be modified as

$$\boldsymbol{K}_{\text{mod}} = \boldsymbol{K} + \begin{bmatrix} \frac{1}{3} & \frac{1}{3} & \frac{1}{3} \\ \frac{\sqrt{3}}{3} & \frac{\sqrt{3}}{3} & \frac{\sqrt{3}}{3} \\ 0 & 0 & 0 \end{bmatrix} \tag{A.28}$$

$$= \begin{bmatrix} 1 & 0 & 0 \\ \frac{\sqrt{3}}{3} & \frac{2\sqrt{3}}{3} & 0 \\ \frac{1}{3} & \frac{1}{3} & \frac{1}{3} \end{bmatrix}. \tag{A.29}$$

The modified Clarke transformation gives the same results as the original Clarke transformation when applied to balanced vectors. Thus, one can compute the α and β variables using only a and b variables. Similar modification can be made for the inverse transformation.

The Clarke transformation as defined in (2.55) does not preserve the magnitude of the transformed vectors and is not power invariant. For example, the power dissipated on the phase resistances is

$$P_{\text{res}} = R_{\text{s}} \boldsymbol{i}_{\text{abc}}^{\text{T}} \boldsymbol{i}_{\text{abc}} \tag{A.30}$$

$$= R_{\text{s}} \boldsymbol{i}_{\alpha\beta\gamma}^{\text{T}} \boldsymbol{K}^{-\text{T}} \boldsymbol{K}^{-1} \boldsymbol{i}_{\alpha\beta\gamma} \tag{A.31}$$

$$= \frac{3}{2} R_{\text{s}} \boldsymbol{i}_{\alpha\beta\gamma}^{\text{T}} \boldsymbol{i}_{\alpha\beta\gamma} \tag{A.32}$$

and the factor 3/2 is required when computing actual power using the transformed vectors.

However, the Clarke transformation preserves amplitude of sinusoidal balanced variables.

There are also two other variants of the Clarke transformation defined as

$$\boldsymbol{K}_{\mathrm{v2}} = \sqrt{\frac{2}{3}} \begin{bmatrix} 1 & \cos\left(\frac{2\pi}{3}\right) & \cos\left(-\frac{2\pi}{3}\right) \\ 0 & \sin\left(\frac{2\pi}{3}\right) & \sin\left(-\frac{2\pi}{3}\right) \\ \frac{1}{2} & \frac{1}{2} & \frac{1}{2} \end{bmatrix}, \tag{A.33}$$

$$\boldsymbol{K}_{\mathrm{v3}} = \sqrt{\frac{2}{3}} \begin{bmatrix} 1 & \cos\left(\frac{2\pi}{3}\right) & \cos\left(-\frac{2\pi}{3}\right) \\ 0 & \sin\left(\frac{2\pi}{3}\right) & \sin\left(-\frac{2\pi}{3}\right) \\ \frac{1}{\sqrt{2}} & \frac{1}{\sqrt{2}} & \frac{1}{\sqrt{2}} \end{bmatrix}. \tag{A.34}$$

The transformation $\boldsymbol{K}_{\mathrm{v2}}$ is power invariant for balanced variables and it preserves the magnitude of the transformed balanced vectors. The transformation $\boldsymbol{K}_{\mathrm{v3}}$ is unitary transformation and is power invariant and preserves the magnitude of the transformed vectors even when they are not balanced. As the phase currents and voltages in PMSM are balanced, both transformation result in the same DQ model

$$L_{\mathrm{d}}\frac{\mathrm{d}i_{\mathrm{d}}}{\mathrm{d}t} = -R_{\mathrm{s}}i_{\mathrm{d}} + n_{\mathrm{pp}}\omega L_{\mathrm{q}}i_{\mathrm{q}} + v_{\mathrm{d}}, \tag{A.35}$$

$$L_{\mathrm{q}}\frac{\mathrm{d}i_{\mathrm{q}}}{\mathrm{d}t} = -R_{\mathrm{s}}i_{\mathrm{q}} - n_{\mathrm{pp}}\omega L_{\mathrm{d}}i_{\mathrm{d}} - K_{\mathrm{b}}\omega + v_{\mathrm{q}}, \tag{A.36}$$

$$J\frac{\mathrm{d}\omega}{\mathrm{d}t} = n_{\mathrm{pp}}i_{\mathrm{d}}i_{\mathrm{q}}(L_{\mathrm{d}} - L_{\mathrm{q}}) + K_{\mathrm{b}}i_{\mathrm{q}} - B\omega + \tau_{\mathrm{cog}} + \tau_{\mathrm{ex}}, \tag{A.37}$$

$$\frac{\mathrm{d}\theta}{\mathrm{d}t} = \omega, \tag{A.38}$$

where

$$K_{\mathrm{b}} = \sqrt{\frac{3}{2}} n_{\mathrm{pp}}\, \Psi_{\mathrm{m}} \tag{A.39}$$

and other parameters are defined in the same way as in the case of the original Clarke transformation. Thus, care should be taken to have consistency in the used DQ model, Clarke transformation, and the definition of the parameters.

A.3 Star PMSM Equivalent to Delta PMSM

To obtain star-connected equivalent of delta-connected PMSM, the phase variables of delta-connected PMSM are transformed to the source variables and denoted as $\boldsymbol{i}_{\mathrm{abc}\star}$, $\boldsymbol{v}_{\mathrm{abc}\star}$, which are interpreted as the phase variables of a star-connected PMSM It is tehn shown that the model of delta-connected PMSM expressed in the transformed vectors is equivalent to model of star-connected PMSM. The transformations are as in subsection 2.2.5 and the following

forms are used

$$\boldsymbol{i}_{\mathrm{abc}} = \boldsymbol{K}_{\mathrm{sc}\to\mathrm{pc}}\boldsymbol{i}_{\mathrm{abc}\star}, \tag{A.40}$$

$$\boldsymbol{v}_{\mathrm{abc}\star} = \boldsymbol{K}_{\mathrm{pv}\to\mathrm{sv}}\boldsymbol{v}_{\mathrm{abc}}, \tag{A.41}$$

where

$$\boldsymbol{K}_{\mathrm{sc}\to\mathrm{pc}} = \frac{1}{3}\begin{bmatrix} 1 & -1 & 0 \\ 0 & 1 & -1 \\ -1 & 0 & 1 \end{bmatrix}, \tag{A.42}$$

$$\boldsymbol{K}_{\mathrm{pv}\to\mathrm{sv}} = \frac{1}{3}\begin{bmatrix} 1 & 0 & -1 \\ -1 & 1 & 0 \\ 0 & -1 & 1 \end{bmatrix} \tag{A.43}$$

and the common-mode voltage of $\boldsymbol{v}_{\mathrm{abc}\star}$ was set to zero. The subscript sc $\to$ pc stands for the transformation of source currents to phase currents. The subscript pv $\to$ sv stands for the transformation of phase voltages to source voltages. It is worth noting that

$$\boldsymbol{K}_{\mathrm{sc}\to\mathrm{pc}} = \boldsymbol{K}_{\mathrm{pv}\to\mathrm{sv}}^{\mathrm{T}}. \tag{A.44}$$

Further, star-equivalent back EMF is defined as

$$\boldsymbol{e}_{\mathrm{abc}\star} = \boldsymbol{K}_{\mathrm{pv}\to\mathrm{sv}}\boldsymbol{e}_{\mathrm{abc}}. \tag{A.45}$$

The voltage equation (2.48) is transformed by substituting in for the phase currents and then multiplying by $\boldsymbol{K}_{\mathrm{vp}\to\mathrm{vs}}$ from the left. The mechanical equation (2.49) is transformed by substituting in for the phase currents. This results in

$$\boldsymbol{L}_\star\frac{\mathrm{d}\boldsymbol{i}_{\mathrm{abc}\star}}{\mathrm{d}t} = -\boldsymbol{R}_{\mathrm{s}\star}\boldsymbol{i}_{\mathrm{abc}\star} - \omega\boldsymbol{L}'_\star\boldsymbol{i}_{\mathrm{abc}\star} - \boldsymbol{e}_{\mathrm{abc}\star} + \boldsymbol{v}_{\mathrm{abc}\star}, \tag{A.46}$$

$$J\frac{\mathrm{d}\omega}{\mathrm{d}t} = \frac{1}{2}\boldsymbol{i}_{\mathrm{abc}\star}^{\mathrm{T}}\boldsymbol{L}'_\star\boldsymbol{i}_{\mathrm{abc}\star} + \frac{1}{\omega}\boldsymbol{i}_{\mathrm{abc}\star}^{\mathrm{T}}\boldsymbol{e}_{\mathrm{abc}\star} - B\omega + \tau_{\mathrm{cog}} + \tau_{\mathrm{ex}}, \tag{A.47}$$

$$\frac{\mathrm{d}\theta}{\mathrm{d}t} = \omega \tag{A.48}$$

where

$$\boldsymbol{R}_{\mathrm{s}\star} = \boldsymbol{K}_{\mathrm{pv}\to\mathrm{sv}}R_{\mathrm{s}}\boldsymbol{K}_{\mathrm{sc}\to\mathrm{pc}}, \tag{A.49}$$

$$\boldsymbol{L}_\star = \boldsymbol{K}_{\mathrm{pv}\to\mathrm{sv}}\boldsymbol{L}\boldsymbol{K}_{\mathrm{sc}\to\mathrm{pc}}, \tag{A.50}$$

$$\boldsymbol{L}'_\star = \boldsymbol{K}_{\mathrm{pv}\to\mathrm{sv}}\boldsymbol{L}'\boldsymbol{K}_{\mathrm{sc}\to\mathrm{pc}}. \tag{A.51}$$

Now the rotor angle is transformed to $\theta_\star$ by defining

$$\theta_\star \;=\; \theta + \frac{1}{n_{\mathrm{pp}}}\left(\frac{\pi}{3} - \frac{\pi}{2}\right). \tag{A.52}$$

The transformation of the rotor angle is required because $\boldsymbol{i}_{\mathrm{abc}\star}$ are the source currents of the delta-connected PMSM, not the phase currents. The equations (A.46), (A.47), and (A.48) expressed in $\theta_\star$ are then transformed to DQ model using Clarke and Park transformations. This gives star-equivalent DQ model

$$\begin{aligned}
L_{\mathrm{d}\star}\frac{\mathrm{d}i_{\mathrm{d}\star}}{\mathrm{d}t} &= -R_{\mathrm{s}\star}i_{\mathrm{d}\star} + n_{\mathrm{pp}}\omega L_{\mathrm{q}\star}i_{\mathrm{q}\star} + v_{\mathrm{d}\star}, && \text{(A.53)}\\
L_{\mathrm{q}\star}\frac{\mathrm{d}i_{\mathrm{q}\star}}{\mathrm{d}t} &= -R_{\mathrm{s}\star}i_{\mathrm{q}\star} - n_{\mathrm{pp}}\omega L_{\mathrm{d}\star}i_{\mathrm{d}\star} - K_{\mathrm{b}\star}\omega + v_{\mathrm{q}\star}, && \text{(A.54)}\\
J\frac{\mathrm{d}\omega}{\mathrm{d}t} &= \frac{3}{2}n_{\mathrm{pp}}i_{\mathrm{d}\star}i_{\mathrm{q}\star}(L_{\mathrm{d}\star} - L_{\mathrm{q}\star}) + \frac{3}{2}K_{\mathrm{b}\star}i_{\mathrm{q}\star} - B\omega + \tau_{\mathrm{cog}} + \tau_{\mathrm{ex}}, && \text{(A.55)}\\
\frac{\mathrm{d}\theta_\star}{\mathrm{d}t} &= \omega, && \text{(A.56)}
\end{aligned}$$

where

$$\begin{aligned}
R_{\mathrm{s}\star} &= \frac{1}{3}R_{\mathrm{s}}, && \text{(A.57)}\\
L_{\mathrm{d}\star} &= \frac{1}{3}\left(L_{\mathrm{s}} + M_{\mathrm{s}} + \frac{3}{2}L_{\mathrm{g}}\right) \;=\; \frac{1}{3}L_{\mathrm{d}}, && \text{(A.58)}\\
L_{\mathrm{q}\star} &= \frac{1}{3}\left(L_{\mathrm{s}} + M_{\mathrm{s}} - \frac{3}{2}L_{\mathrm{g}}\right) \;=\; \frac{1}{3}L_{\mathrm{q}}, && \text{(A.59)}\\
K_{\mathrm{b}\star} &= \frac{\sqrt{3}}{3}n_{\mathrm{pp}}\,\Psi_{\mathrm{m}} \;=\; \frac{\sqrt{3}}{3}K_{\mathrm{b}}. && \text{(A.60)}
\end{aligned}$$

Thus, delta-connected PMSM is equivalent to a star-connected PMSM with parameters scaled as shown above.

Appendix B

MPC in Condensed Form

The MPC control task (3.11) is reformulated to condensed form by defining

$$\boldsymbol{X} = \begin{bmatrix} \boldsymbol{x}_1^{\mathrm{T}} & \boldsymbol{x}_2^{\mathrm{T}} & \dots & \boldsymbol{x}_N^{\mathrm{T}} \end{bmatrix}^{\mathrm{T}}, \tag{B.1}$$

$$\boldsymbol{Y} = \begin{bmatrix} \boldsymbol{y}_1^{\mathrm{T}} & \boldsymbol{y}_2^{\mathrm{T}} & \dots & \boldsymbol{y}_N^{\mathrm{T}} \end{bmatrix}^{\mathrm{T}}, \tag{B.2}$$

$$\boldsymbol{U} = \begin{bmatrix} \boldsymbol{u}_0^{\mathrm{T}} & \boldsymbol{u}_1^{\mathrm{T}} & \dots & \boldsymbol{u}_{N-1}^{\mathrm{T}} \end{bmatrix}^{\mathrm{T}}, \tag{B.3}$$

$$\Delta\boldsymbol{U} = \begin{bmatrix} \Delta\boldsymbol{u}_0^{\mathrm{T}} & \Delta\boldsymbol{u}_1^{\mathrm{T}} & \dots & \Delta\boldsymbol{u}_{N-1}^{\mathrm{T}} \end{bmatrix}^{\mathrm{T}}, \tag{B.4}$$

$$\boldsymbol{Y}^* = \begin{bmatrix} \boldsymbol{r}_1^{\mathrm{T}} & \boldsymbol{r}_2^{\mathrm{T}} & \dots & \boldsymbol{r}_N^{\mathrm{T}} \end{bmatrix}^{\mathrm{T}}. \tag{B.5}$$

Using these vectors, the cost function in (3.11a) can be expressed as

$$J = (\boldsymbol{Y}^* - \boldsymbol{Y})^{\mathrm{T}} \overline{\boldsymbol{Q}} (\boldsymbol{Y}^* - \boldsymbol{Y}) + \Delta\boldsymbol{U}^{\mathrm{T}} \overline{\boldsymbol{R}} \Delta\boldsymbol{U}, \tag{B.6}$$

where

$$\overline{\boldsymbol{Q}} = \begin{bmatrix} \boldsymbol{Q} & \boldsymbol{0} & \cdots & \\ \boldsymbol{0} & \boldsymbol{Q} & & \\ \vdots & & \ddots & \\ & & & \boldsymbol{Q} \end{bmatrix}, \qquad \overline{\boldsymbol{R}} = \begin{bmatrix} \boldsymbol{R} & \boldsymbol{0} & \cdots & \\ \boldsymbol{0} & \boldsymbol{R} & & \\ \vdots & & \ddots & \\ & & & \boldsymbol{R} \end{bmatrix}. \tag{B.7}$$

Equations describing the model (3.11b) and (3.11c) are rewritten as

$$\boldsymbol{X} = \overline{\boldsymbol{A}}\boldsymbol{x}_0 + \overline{\boldsymbol{B}}\boldsymbol{U}, \tag{B.8}$$

$$\boldsymbol{Y} = \overline{\boldsymbol{C}}\boldsymbol{X}, \tag{B.9}$$

where

$$\overline{\boldsymbol{A}} = \begin{bmatrix} \boldsymbol{A} \\ \boldsymbol{A}^2 \\ \boldsymbol{A}^3 \\ \vdots \\ \boldsymbol{A}^N \end{bmatrix}, \qquad \overline{\boldsymbol{B}} = \begin{bmatrix} \boldsymbol{B} & \boldsymbol{0} & \boldsymbol{0} & \cdots & \\ \boldsymbol{AB} & \boldsymbol{B} & \boldsymbol{0} & \cdots & \\ \boldsymbol{A}^2\boldsymbol{B} & \boldsymbol{AB} & \boldsymbol{B} & \cdots & \\ \vdots & \vdots & \vdots & \ddots & \\ \boldsymbol{A}^{N-1}\boldsymbol{B} & \boldsymbol{A}^{N-2}\boldsymbol{B} & \boldsymbol{A}^{N-3}\boldsymbol{B} & \cdots & \boldsymbol{B} \end{bmatrix}, \tag{B.10}$$

$$\overline{\boldsymbol{C}} = \begin{bmatrix} \boldsymbol{C} & \boldsymbol{0} & \cdots & \\ \boldsymbol{0} & \boldsymbol{C} & & \\ \vdots & & \ddots & \\ & & & \boldsymbol{C} \end{bmatrix}. \tag{B.11}$$

Vector $\Delta\boldsymbol{U}$ can be expressed as

$$\Delta\boldsymbol{U} = \overline{\boldsymbol{S}}\boldsymbol{U} - \overline{\boldsymbol{E}}\boldsymbol{u}_{-1}, \tag{B.12}$$

where

$$\overline{\boldsymbol{S}} = \begin{bmatrix} \boldsymbol{I} & \boldsymbol{0} & \boldsymbol{0} & \cdots & \\ -\boldsymbol{I} & \boldsymbol{I} & \boldsymbol{0} & & \\ \boldsymbol{0} & -\boldsymbol{I} & \boldsymbol{I} & & \\ \vdots & & & \ddots & \\ & & & & \boldsymbol{I} \end{bmatrix}, \qquad \overline{\boldsymbol{E}} = \begin{bmatrix} \boldsymbol{I} \\ \boldsymbol{0} \\ \boldsymbol{0} \\ \vdots \\ \boldsymbol{0} \end{bmatrix}. \tag{B.13}$$

The dimensions of identity matrix $\boldsymbol{I}$ are $n_u \times n_u$, where $n_u = 2$ is the number of inputs.

Using (B.8), (B.9), and (B.12), the cost function (B.6) is rewritten as

$$\begin{aligned} J = {} & (\boldsymbol{Y}^* - \overline{\boldsymbol{C}}\overline{\boldsymbol{A}}\boldsymbol{x}_0 - \overline{\boldsymbol{C}}\overline{\boldsymbol{B}}\boldsymbol{U})^{\mathrm{T}}\overline{\boldsymbol{Q}}(\boldsymbol{Y}^* - \overline{\boldsymbol{C}}\overline{\boldsymbol{A}}\boldsymbol{x}_0 - \overline{\boldsymbol{C}}\overline{\boldsymbol{B}}\boldsymbol{U}) \\ & + (\overline{\boldsymbol{S}}\boldsymbol{U} - \overline{\boldsymbol{E}}\boldsymbol{u}_{-1})^{\mathrm{T}}\overline{\boldsymbol{R}}(\overline{\boldsymbol{S}}\boldsymbol{U} - \overline{\boldsymbol{E}}\boldsymbol{u}_{-1}). \end{aligned} \tag{B.14}$$

Expanding, rearranging, and using the fact that $\overline{\boldsymbol{Q}}$ and $\overline{\boldsymbol{R}}$ are symmetric

$$J = \frac{1}{2}\boldsymbol{U}^{\mathrm{T}}\boldsymbol{H}\boldsymbol{U} + \overline{\boldsymbol{F}}^{\mathrm{T}}\boldsymbol{U} + c, \tag{B.15}$$

where

$$\boldsymbol{H} = 2\left(\overline{\boldsymbol{B}}^{\mathrm{T}}\overline{\boldsymbol{C}}^{\mathrm{T}}\overline{\boldsymbol{Q}}\overline{\boldsymbol{C}}\overline{\boldsymbol{B}} + \overline{\boldsymbol{S}}^{\mathrm{T}}\overline{\boldsymbol{R}}\overline{\boldsymbol{S}}\right), \tag{B.16}$$

$$\overline{\boldsymbol{F}}^{\mathrm{T}} = 2\left(\boldsymbol{x}_0^{\mathrm{T}}\overline{\boldsymbol{A}}^{\mathrm{T}}\overline{\boldsymbol{C}}^{\mathrm{T}}\overline{\boldsymbol{Q}}\overline{\boldsymbol{C}}\overline{\boldsymbol{B}} - \boldsymbol{u}_{-1}^{\mathrm{T}}\overline{\boldsymbol{E}}^{\mathrm{T}}\overline{\boldsymbol{R}}\overline{\boldsymbol{S}} - \boldsymbol{Y}^{*\mathrm{T}}\overline{\boldsymbol{Q}}\overline{\boldsymbol{C}}\overline{\boldsymbol{B}}\right), \tag{B.17}$$

$$c = \left(\boldsymbol{Y}^{*\mathrm{T}} - \overline{\boldsymbol{C}}\overline{\boldsymbol{A}}\boldsymbol{x}_0\right)^{\mathrm{T}}\overline{\boldsymbol{Q}}\left(\boldsymbol{Y}^{*\mathrm{T}} - \overline{\boldsymbol{C}}\overline{\boldsymbol{A}}\boldsymbol{x}_0\right) + \boldsymbol{u}_{-1}^{\mathrm{T}}\overline{\boldsymbol{E}}^{\mathrm{T}}\overline{\boldsymbol{R}}\overline{\boldsymbol{E}}\boldsymbol{u}_{-1}. \tag{B.18}$$

Further

$$J = \frac{1}{2}\boldsymbol{U}^{\mathrm{T}}\boldsymbol{H}\boldsymbol{U} + \begin{bmatrix}\boldsymbol{x}_0^{\mathrm{T}} & \boldsymbol{u}_{-1}^{\mathrm{T}} & \boldsymbol{Y}^{*\mathrm{T}}\end{bmatrix}\boldsymbol{F}^{\mathrm{T}}\boldsymbol{U} + c, \tag{B.19}$$

where

$$\boldsymbol{F}^{\mathrm{T}} = \begin{bmatrix} 2\overline{\boldsymbol{A}}^{\mathrm{T}}\overline{\boldsymbol{C}}^{\mathrm{T}}\overline{\boldsymbol{Q}}\overline{\boldsymbol{C}}\overline{\boldsymbol{B}} \\ -2\overline{\boldsymbol{E}}^{\mathrm{T}}\overline{\boldsymbol{R}}\overline{\boldsymbol{S}} \\ -2\overline{\boldsymbol{Q}}\overline{\boldsymbol{C}}\overline{\boldsymbol{B}} \end{bmatrix}. \tag{B.20}$$

As c is a constant that does not depend on the optimization variable $\boldsymbol{U}$, it does not influence the solution of the optimization problem. Thus,

$$\tilde{J} = \frac{1}{2}\boldsymbol{U}^{\mathrm{T}}\boldsymbol{H}\boldsymbol{U} + \begin{bmatrix}\boldsymbol{x}_0^{\mathrm{T}} & \boldsymbol{u}_{-1}^{\mathrm{T}} & \boldsymbol{Y}^{*\mathrm{T}}\end{bmatrix}\boldsymbol{F}^{\mathrm{T}}\boldsymbol{U} \tag{B.21}$$

has the same minimizer as J.

The inequality constraints (3.11d) and (3.11e) are rewritten as

$$\overline{\boldsymbol{P}}_x\boldsymbol{X} \leq \bar{\boldsymbol{p}}_x, \tag{B.22}$$

$$\overline{\boldsymbol{P}}_u\boldsymbol{U} \leq \bar{\boldsymbol{p}}_u, \tag{B.23}$$

where

$$\overline{\boldsymbol{P}}_x = \begin{bmatrix} \boldsymbol{P}_x & \boldsymbol{0} & \cdots & \\ \boldsymbol{0} & \boldsymbol{P}_x & & \\ \vdots & & \ddots & \\ & & & \boldsymbol{P}_x \end{bmatrix}, \quad \bar{\boldsymbol{p}}_x = \begin{bmatrix} \boldsymbol{p}_x \\ \boldsymbol{p}_x \\ \vdots \\ \boldsymbol{p}_x \end{bmatrix}, \tag{B.24}$$

$$\overline{\boldsymbol{P}}_u = \begin{bmatrix} \boldsymbol{P}_u & \boldsymbol{0} & \cdots & \\ \boldsymbol{0} & \boldsymbol{P}_u & & \\ \vdots & & \ddots & \\ & & & \boldsymbol{P}_u \end{bmatrix}, \quad \bar{\boldsymbol{p}}_u = \begin{bmatrix} \boldsymbol{p}_u \\ \boldsymbol{p}_u \\ \vdots \\ \boldsymbol{p}_u \end{bmatrix}. \tag{B.25}$$

Using (B.8) the constraint (B.22) is rewritten as

$$\overline{\boldsymbol{P}}_x\overline{\boldsymbol{B}}\boldsymbol{U} \;\leq\; \bar{\boldsymbol{p}}_x - \overline{\boldsymbol{P}}_x\overline{\boldsymbol{A}}\boldsymbol{x}_0. \tag{B.26}$$

Combining (B.23) and (B.26) gives

$$\boldsymbol{G}\boldsymbol{U} \;\leq\; \boldsymbol{W} + \boldsymbol{S}\boldsymbol{x}_0, \tag{B.27}$$

where

$$\boldsymbol{G} \;=\; \begin{bmatrix} \overline{\boldsymbol{P}}_x\overline{\boldsymbol{B}} \\ \overline{\boldsymbol{P}}_u \end{bmatrix}, \qquad \boldsymbol{W} = \begin{bmatrix} \bar{\boldsymbol{p}}_x \\ \bar{\boldsymbol{p}}_u \end{bmatrix}, \qquad \boldsymbol{S} \;=\; \begin{bmatrix} -\overline{\boldsymbol{P}}_x\overline{\boldsymbol{A}} \\ \boldsymbol{0} \end{bmatrix}. \tag{B.28}$$

Therefore, MPC control task can be written in condensed form as

$$\min_{\boldsymbol{z}} \quad \frac{1}{2}\boldsymbol{z}^{\mathrm{T}}\boldsymbol{H}\boldsymbol{z} + \begin{bmatrix} \boldsymbol{x}_0^{\mathrm{T}} & \boldsymbol{u}_{-1}^{\mathrm{T}} & \boldsymbol{r}_1^{\mathrm{T}} & \boldsymbol{r}_2^{\mathrm{T}} & \dots & \boldsymbol{r}_N^{\mathrm{T}} \end{bmatrix} \boldsymbol{F}^{\mathrm{T}}\boldsymbol{z} \tag{B.29a}$$

$$\text{s.t.} \quad \boldsymbol{G}\boldsymbol{z} \;\leq\; \boldsymbol{W} + \boldsymbol{S}\boldsymbol{x}_0, \tag{B.29b}$$

$$\boldsymbol{z} \;=\; \begin{bmatrix} \boldsymbol{u}_0^{\mathrm{T}} & \boldsymbol{u}_1^{\mathrm{T}} & \dots & \boldsymbol{u}_{N-1^{\mathrm{T}}} \end{bmatrix}^{\mathrm{T}}, \tag{B.29c}$$

$$\boldsymbol{x}_0 \;=\; \boldsymbol{x}(t), \tag{B.29d}$$

$$\boldsymbol{u}_{-1} \;=\; \boldsymbol{u}(t - T_{\mathrm{s}}), \tag{B.29e}$$

$$\boldsymbol{r}_k \;=\; \boldsymbol{r}(t + kT_{\mathrm{s}}), \quad k \;=\; 1,\, 2,\, \dots,\, N. \tag{B.29f}$$

.

Bibliography

[1] Paul Krause, Oleg Wasynczuk, Scott D. Sudhoff, et al. *Analysis of Electric Machinery and Drive Systems*. Third Edition. Wiley-IEEE Press, 2013. ISBN: 978-1-118-02429-4.

[2] G. Cimini, D. Bernardini, A. Bemporad, et al. "Online model predictive torque control for Permanent Magnet Synchronous Motors". In: *2015 IEEE International Conference on Industrial Technology (ICIT)*. Mar. 2015, pp. 2308–2313. DOI: 10.1109/ICIT.2015.7125438.

[3] A. A. Ahmed, B. K. Koh, and Y. I. Lee. "A Comparison of Finite Control Set and Continuous Control Set Model Predictive Control Schemes for Speed Control of Induction Motors". In: *IEEE Transactions on Industrial Informatics* 14.4 (Mar. 2018), pp. 1334–1346. ISSN: 1557-9948. DOI: 10.1109/TIE.2016.2631456.

[4] S. Vazquez, J. I. Leon, L. G. Franquelo, et al. "Model Predictive Control: A Review of Its Applications in Power Electronics". In: *IEEE Industrial Electronics Magazine* 8.1 (Mar. 2014), pp. 16–31. ISSN: 1932-4529. DOI: 10.1109/MIE.2013.2290138.

[5] Dr. Duane Hanselman. *Brushless Permanent Magnet Motor Design*. Second Edition. Magna Physics Publishing, 2006. ISBN: 1-881855-15-5.

[6] John Chiasson. *Modeling and High-Performance Control of Electric Machines*. John Wiley & Sons, 2005. ISBN: 0-471-68449-X.

[7] Fouad Giri. *AC Electric Motors Control: Advanced Design Techniques and Applications*. John Wiley & Sons, 2013. ISBN: 978-1-118-33152-1.

[8] N. Moehle and S. Boyd. "Optimal current waveforms for brushless permanent magnet motors". In: *International Journal of Control* 88.7 (2015), pp. 1389–1399. DOI: 10.1080/00207179.2015.1012558. eprint: https://doi.org/10.1080/00207179.2015.1012558. URL: https://doi.org/10.1080/00207179.2015.1012558.

[9] J. Rodriguez, M. P. Kazmierkowski, J. R. Espinoza, et al. "State of the Art of Finite Control Set Model Predictive Control in Power Electronics". In: *IEEE Transactions on Industrial Informatics* 9.2 (May 2013), pp. 1003–1016. ISSN: 1551-3203. DOI: 10.1109/TII.2012.2221469.

[10] Jose Rodriguez and Patricio Cortes. *Predictive Control of Power Converters and Electrical Drives*. Wiley-IEEE Press, 2012. ISBN: 978-1-119-96398-1.

[11] Tobias Geyer. *Model Predictive Control of High Power Converters and Industrial Drives*. John Wiley & Sons, 2017. ISBN: 978-1-119-01086-9.

[12] Ramu Krishnan. *Permanent Magnet Synchronous and Brushless DC Motor Drives*. CRC Press, Taylor & Francis Group, 2010. ISBN: 978-0-8247-5384-9.

[13] K. Belda and L. Pavelkova. “Online tuned model predictive control for robotic systems with bounded noise”. In: *2017 22nd International Conference on Methods and Models in Automation and Robotics (MMAR)*. 2017, pp. 694–699.

[14] Anaheim Automation. *BLWR23 Series - Brushless DC Motors*. Product Sheet. URL: https://www.anaheimautomation.com/manuals/brushless/L010231%20-%20BLWR23%20Series%20Product%20Sheet.pdf (visited on 08/05/2020).

[15] Viktor Bobek. *PMSM Electrical Parameters Measurement*. Application Note, Document Number: AN4680, Rev. 0. Freescale Semiconductor, Feb. 2013. URL: https://www.nxp.com/docs/en/application-note/AN4680.pdf.

[16] P. Václavek and P. Blaha. “Field weakening in PMSM model based predictive control”. In: *2010 IEEE International Conference on Power and Energy*. 2010, pp. 330–335.

[17] Z. Mynar, L. Vesely, and P. Vaclavek. “PMSM Model Predictive Control With Field-Weakening Implementation”. In: *IEEE Transactions on Industrial Electronics* 63.8 (2016), pp. 5156–5166.

[18] Luca Corradini, Dragan Maksimović, Paolo Mattavelli, et al. *Digital Control of High-Frequency Switched-Mode Power Converters*. Wiley-IEEE Press, 2015. ISBN: 978-1-118-93510-1.

[19] D. G. Holmes. “The general relationship between regular-sampled pulse-width-modulation and space vector modulation for hard switched converters”. In: *Conference Record of the 1992 IEEE Industry Applications Society Annual Meeting*. 1992, 1002–1009 vol.1.

[20] A Linder, Rahul Kanchan, Ralph Kennel, et al. *Model-Based Predictive Control of Electric Drives*. Jan. 2012. ISBN: 978-3869553986.